Title
THE STRUCTURE OF ADSORBED MONOLAYERS. THE SURFACE CHEMICAL BOND

Authors
Somorjai, G.A.
Bent, B.E.

Publication Date
1984-06-01

Lawrence Berkeley Laboratory
UNIVERSITY OF CALIFORNIA

Materials & Molecular Research Division

Presented at the 8th Scandinavian Symposium on Surface Chemistry, Chemical Center, University of Lund, Lund, Sweden, June 4-6, 1984

THE STRUCTURE OF ADSORBED MONOLAYERS. THE SURFACE CHEMICAL BOND

G.A. Somorjai and B.E. Bent

June 1984

Prepared for the U.S. Department of Energy under Contract DE-AC03-76SF00098

DISCLAIMER

LBL#18011

THE STRUCTURE OF ADSORBED MONOLAYERS. THE SURFACE CHEMICAL BOND.

G.A. Somorjai and B.E. Bent

Materials and Molecular Research Division,
Lawrence Berkeley Laboratory and
Department of Chemistry
University of California
Berkeley, California 94720, USA

1. Introduction

During the last fifteen years new techniques developed by modern surface science have permitted a molecular level scrutiny of the surface monolayer.(1) Table I lists many of the techniques utilized most frequently in molecular surface science studies. Most of these surface science techniques utilize electron or ion scattering and require a change of density at the interface for surface sensitivity. As a result, most studies have been performed at the solid-vacuum and solid-gas interfaces and not at solid-liquid interfaces.

Using these techniques, the atomic surface structures of clean surfaces and adsorbate monolayers have been determined. Surface composition can be verified to better than 1% of a monolayer (10^{13} atoms/cm^2 or less). The oxidation states of surface atoms can also now be verified.

This paper attempts to provide a summary of what has been learned about the structure of adsorbed monolayers and about the surface chemical bond from molecular surface science. While the surface chemical bond is less well understood than bonding of molecules in the gas phase or in the solid state, our knowledge of its properties is rapidly accumulating. The information obtained also has great impact on many surface science based technologies, including heterogeneous catalysis and electronic devices. It is hoped that much of the information obtained from studies at solid-gas interfaces can be correlated with molecular behavior at solid-liquid interfaces.

1.1 Surface Science Technology

Figure 1 shows the experimental geometry that is usually used in modern surface science studies.(1) A sample, usually a single crystal of

about 1 cm^2 surface area, is enclosed by an ultra-high vacuum chamber, and there are various surface techniques surrounding it. Surface cleaning is carried out by ion bombardment and the surface orientation and structure are tested by low energy electron diffraction. Electron spectroscopies, including photoelectron spectroscopy and Auger electron spectroscopy, determine the surface composition and the oxidation state of surface atoms. High resolution electron energy loss spectroscopy is used to study the vibrational structure of atoms or molecules adsorbed on surfaces.

Figure 2 shows the power of a single electron beam in determining many of the surface chemical properties.(2) An incident electron beam of a few hundred or a thousand electron volts in energy yields an elastically scattered fraction that is used for low energy electron diffraction and surface crystallography to determine the precise location of atoms -- their bond distances and bond angles.(3) Very minute energy losses in the milli-electron volt range result from excitation of surface vibrations and provide an assignable surface vibrational spectrum.(4) Energy losses due to inner shell excitation or deexcitation processes give rise to photoelectron spectra(5) and Auger electron spectra(6).

1.2 Surface Composition

Knowing the surface composition is necessary for surface structure determinations. An example of the Auger electron spectra used to determine surface composition is exhibited in Figure 3 for a silver-gold alloy.(7) From the Auger peak height ratios, the silver to gold surface atom ratios were determined. It is found that there is surface segregation of one of the constituents, in this case silver, due to surface thermodynamic reasons. The surface composition is adjusted to minimize the total surface

energy, thereby segregating to the surface that constituent of lower surface energy, in this case silver. Surface composition studies is a function of depth (depth profile analysis) clearly reveal changes of surface composition layer by layer from the surface inward. This is shown in Figure 4. The surface layer has excess of silver relative to the bulk silver-gold alloy composition, the second layer has excess gold, the third layer has excess silver again, and by the fourth layer the bulk composition is achieved.

Figure 5 shows the regular solution and ideal solid solution equations that govern surface segregation for two component systems.(8) Here σ_1 and σ_2 are the surface tensions of the pure component 1 and 2, X_1^s and X_2^s are the atom fractions of the two components at the surface, and X_1^b and X_2^b are the atom fractions of the two components in the bulk. Ω is a regular solution parameter that is proportional to the heat of mixing as shown in Figure 5. Clearly, that component that has the lower surface tension or surface free energy is segregated to the surface exponentially in the surface tension difference. It should also be noted that the surface composition is temperature dependent.

2. Structure of Clean Solid Surfaces

2.1 Surface Site Geometries

Before we scrutinize the surface chemical bond and surface structure of adsorbed monolayers, we should review what has been learned about the structure of clean solid surfaces. Figure 6 shows a schematic diagram of a typical surface. Surfaces on an atomic scale are heterogeneous. The various sites are distinguishable by their number of nearest neighbors. Atoms in terraces have the largest number of nearest neighbors; at steps

and ledges they have lower coordination. There is experimental evidence for the presence of all of these surface sites.

Let us concentrate on the structure of these various surfaces, the prototypes of which are shown in Figure 7. There are flat surfaces which are low-Miller-index, single-crystal surfaces of cubic materials that have six or four atoms as nearest neighbors in the surface layer. Most surface science studies have been carried out on these flat, low-Miller-index surfaces. Then there are stepped surfaces which are the typical structure of high-Miller-index, single-crystal surfaces. Often the steps are also in the direction of high-Miller-index in which case there are ordered ledges in the steps.

2.2 Surface Reconstruction and Relaxation

Let us first concentrate on the surfaces of flat, low-Miller-index planes. Figure 8 shows the (100) crystal face of platinum. When clean, this surface is reconstructed and its diffraction pattern indicates the presence of a 5 x 20 surface structure. When the surface is impure or has a fraction of a monolayer of adsorbates, the square unit cell shown in Figure 8 is obtained, which is what one would expect from projection of the bulk unit cell up to the surface. While this 5x20 surface structure was first detected in our laboratory in 1965(9), it was actually solved by surface crystallography in 1981.(10)

This surface structure, with the location of platinum atoms in the surface shown, is depicted in Figure 9. The surface is reconstructed into an hexagonal, close-packed structure which sits on top of a square-like second layer. The coincidence of atomic positions between atoms in the first layer and second layer gives rise to the complex diffraction pattern

shown in Figure 8. This hexagonal reconstruction increases the atomic density in the surface layer which lowers the surface free energy. In addition, it leads to buckling of the surface which increases the total surface energy. A compromise between close-packing and buckling leads to a minimum surface energy which determines the location of atoms in this surface.

Gold, platinum and iridium (100) crystal faces all show reconstruction.(1) Figure 10 shows the structure of the reconstructed silicon (100) crystal face. In this surface, the silicon atoms form a dimer-like surface structure and there is a relaxation or contraction at the surface layer with respect to the bulk interlayer distance that extends to three layers below the surface.(11) Thus the effect of the surface is felt three layers into the bulk.

Figure 11 shows the beautiful diffraction patterns exhibited by one of the more stable structures on the reconstructed silicon (111) surface. This is the 7 x 7 structure which has a complex unit cell which is still not resolved by surface crystallography. It is hoped that a resolution in this surface will be forthcoming within a year. It should be noted that the silicon (100) and (111) surfaces are frequently used as substrates for electronic circuitries. As a result, the atomic surface structure of these surfaces is of utmost importance in the integrated circuitry technology, since the electronic transport properties are clearly dependent on the location of atoms at the surface.

There are two major findings of modern surface science that were uncovered during studies of clean solid surfaces. These are reconstruction, as was demonstrated for the platinum and silicon crystal surfaces, and

there is also relaxation. During relaxation the atoms are contracted in their interlayer distance near the surface region with respect to the interlayer distance in the bulk. However, the atomic locations in the surface plane (X,Y plane) are unchanged. Thus the major conclusion of these clean surface structural studies is that the atomic locations at the surface are different from what one would expect from the projection of the bulk unit cells to the clean surface.

3. The Locations of Atomic Adsorbates on Solid Surfaces

Over a hundred systems of atomic adsorbates on clean and flat, solid surfaces have been studied. The results indicate that atoms occupy the high symmetry sites, where the next layer of atoms would locate on a growing, single-crystal surface.(1) Some of these atomic positions are shown in Figure 12. On surfaces that exhibit hexagonal symmetry, atoms sit in three-fold sites. On surfaces exhibiting square symmetry, atoms sit in four-fold sites.

There are some unique atomic adsorbate bonding situations that should be mentioned. Small atoms such as hydrogen or nitrogen often like to sit below the surface. For example these two atoms sit under the titanium single crystal surface. In the presence of strong chemical interactions there may also be rearrangement of the substrate layer (such is the case for oxygen on the iron (100) crystal face).

Many industrially important systems involve two metals or metals adsorbed on surfaces of other metals. The method of growth in metal deposition on metals is what one would expect from the studies of atomic adsorbates and is shown in Figure 13. One can follow such crystal growth with low energy electron diffraction. An epitaxial relationship seems to be prevalent for

metals growing on metal surfaces, that is, the adsorbate interatomic distance seems to mimic the substrate interatomic distance. For example gold, which has a five percent larger interatomic distance than platinum, adapts to the platinum interatomic distance when deposited on (110) single crystal surfaces.(12)

Generally, atomic adsorbates seem to covalently bond and sit in high symmetry sites on low-Miller-index, flat surfaces. This is shown in Figure 14, where the atomic distances obtained for adsorbed atoms on single crystal surfaces are compared with atomic distances for solid compounds or for gas phase molecules. The arrows indicate the range of bond lengths that has been observed. This range is clearly within the range of bond lengths observed in both the gas phase and the solid state. Also, the percentage of ionic character of these bonds, as indicated by the charge transfer in Figure 14, is very small. Thus, covalent bonding predominates for most of the cases that have been studied.

4. The Coverage Dependence of Adsorbate Binding at Solid Surfaces

Thermal desorption spectroscopy provides information about the heat of adsorption of atoms and molecules at solid surfaces.(13) When heating the solid at a well defined rate (in the range of 4 - 20°/sec.), there is a specific temperature at which the desorption rate is a maximum and from which the heat of desorption can be obtained. When the thermal desorption spectrum is taken at different surface coverages, as shown for carbon monoxide in Figure 15, one observes a shift in the peak desorption temperature indicating a variation in the heat of adsorption with coverage.

Such a coverage dependence of the heat of adsorption is shown in Figure 16, where the heat of adsorption of carbon monoxide on the palladium

(100) surface is shown as a function of surface coverage. At low coverages, the heat of adsorption remains by and large unchanged. As the coverage reaches about half a monolayer, there is a great drop in the average heat of adsorption per molecule indicating a weakening of the adsorbate substrate bond. This is due to a repulsive interaction between adsorbed carbon monoxide molecules that weakens their bonding to the metal surface.

While in many cases, including adsorbed organic molecules and carbon monoxide, one obtains a repulsive interaction between adsorbed molecules keeping these molecules apart, there are some other cases, including adsorbed hydrogen and oxygen on many metal surfaces, where one obtains an attractive adsorbate-adsorbate interaction that actually increases the average heat of adsorption per molecule at low coverages. Such an attractive interaction also leads to island growth in the adsorbate layer.

Figures 17 and 18 show the two predominant binding states of carbon monoxide adsorbed on solid surfaces.(15,16) These are the bridge sites and top sites. Unlike atoms that always occupy the high symmetry sites with three-fold or four-fold coordination, carbon monoxide prefers two-fold or one-fold coordination on most metal surfaces at low coverages. As the coverage of CO is increased, a surface structure with CO in both top and bridge sites, such as that shown in Figure 19, may form. In this case, because repulsive interaction between molecules, the molecules in top sites move sideways to occupy a pseudo hexagonal structure site that is most stable at these high coverages. Here we notice a balance of the adsorbate-substrate and adsorbate-adsorbate interaction that clearly controls the location of molecules on surfaces.

5. The Structure of Small, Organic Molecules on Solid Surfaces

Surface crystallography, as a result of rapid development of the theory of low energy electron diffraction and low energy electron scattering, is now at a point where it can solve complex surface structures with large unit cells and with many molecules per unit cell. Several of these will be shown below when we exhibit the surface structures of different organic molecules. There are many ordered surface structures that have been discovered, hundreds of them, that change as a function of coverage as well as a function of temperature. The reason for the richness and diversity of two-dimensional surface structural chemistry is what we would call the two dimensional phase approximation. The molecules and atoms adsorbed on surfaces are protected from desorption or diffusion into the bulk by large potential energy barriers, while there is only a small potential energy barrier to movement along the surface. This situation is diagrammed in Figure 20. As a result, rearrangements and ordering of molecules in two dimensions are readily possible within the molecules' long residence time on surfaces.

5.1 Alkenes

Let us turn our attention to the bonding of organic molecules in organic monolayers on solid surfaces. The first molecule whose surface structure was solved was ethylene on flat metal surfaces such as platinum (111) and rhodium (111).(18,19) The structure of the chemisorbed ethylene molecule at room temperature is shown in Figure 21. Ethylene loses a hydrogen, becoming C_2H_3, and rearranges to bond in a three-fold hollow as shown. This species is known as ethylidyne. The carbon atom closest to the surface has a metal-carbon distance of 2.0Å, shorter than the 2.2Å covalent metal-carbon bond predicted using covalent radii of the atoms.

The carbon-carbon bond is perpendicular to the surface and is stretched to a single bond length.

The same structure is proven by parallel high resolution electron energy loss spectroscopy studies, and Figure 22 shows the vibrational spectrum of adsorbed ethylidyne molecules on the rhodium (111) crystal face.(20) The C_{3v} symmetry determined from peak intensities and the vibrational frequencies clearly coincides with the structure obtained by surface crystallography. The remarkable agreement between the vibrational frequencies for ethylidyne on the surface and ethylidyne in an organometallic, tri-metal cluster $[(CCH_3)Co_3(CO)_9]$ indicates that a localized bonding model can accurately describe the surface bonding of organic fragments.(21)

Figure 23 shows the similar alkylidyne structures of chemisorbed propylene and butenes that have also been found to exist on the (111) crystal faces of platinum, rhodium and palladium. It appears that alkylidyne structures predominate in the bonding of small alkenes on transition metal surfaces at room temperature.

5.2 Benzene

Figure 24 shows the surface structure of benzene on the rhodium (111) crystal face.(22) There are several ordered surface structures that change with coverage. This is one of those. Clearly, benzene lies with its π ring parallel to the surface in this high symmetry structure. Figure 25 shows the vibrational spectrum of benzene chemisorbed with this surface structure. Again, the high symmetry structure is proven by at least two techniques -- low energy electron diffraction and high resolution electron loss spectroscopy.

5.3 Alkanes

Alkanes may be associatively adsorbed on metal surfaces . Figure 26 shows the ordering and structures of alkanes deposited on metal surfaces as a function of temperature.(23) As the adsorption temperature is decreased, these molecules form first a disordered, then an ordered monolayer. As the temperature is lowered still further in the presence of the organic vapor, condensation occurs leading to crystal growth of an organic single crystal. In this way, not only adsorbed monolayers, but also growing crystals of adsorbates can be studied by surface crystallography.

6. Coadsorption of Atoms and Molecules on Solid Surfaces

6.1 Site-blocking: S + H_2 on Mo(100)

It is frequently important to study the presence of two or more atoms or molecules that are simultaneously adsorbed on solid surfaces. There are some cases where the adsorption of one atom blocks the adsorption of the other one. This is the case for the adsorption of hydrogen on a molybdenum (100) surface that is partially covered with sulfur as shown in Figure 27.(24) Here the binding of hydrogen is unaffected by the coadsorption of sulfur. However, the amount of hydrogen that is adsorbed declines rapidly with sulfur coverage. This rapid decline in hydrogen adsorption occurs because every sulfur atom removes the adsorption possibility for two hydrogen atoms which require unoccupied, adjacent sites for adsorption.

6.2 Electronic Interaction: K + CO on Pt(111) and Rh(111)

Interaction between adsorbates is much stronger in the coadsorption of potassium atoms and carbon monoxide on transition metal surfaces. When potassium is adsorbed on a transition metal surface at low coverages, it is completely ionized by charged transfer to the transition metal. When carbon monoxide is coadsorbed with potassium (14), the bonding of carbon monoxide to the metal is substantially strengthened through the strengthening of the metal-carbon bond, while the carbon oxygen bond is substantially weakened, increasing the probability for the dissociation of carbon monoxide.

This bonding change is exhibited in Figure 28 where the vibrational spectrum of carbon monoxide on Pt(111) with increasing concentration of potassium is shown.(25) This Figure clearly shows the weakening of the carbon-oxygen bond by the shift in the CO stretching frequency to lower energy. The bond-weakening amounts to a change from a CO double bond to a one and a half bond on this platinum surface. This electronic interaction between adsorbates can be explained by the molecular orbital diagram shown in Figure 29. Charges from the potassium change the density of states of electrons at the fermi level in the transition metal. These electrons from the transition metal in turn find their way to antibonding and bonding molecular orbitals of the coadsorbed organic molecules, in this case carbon monoxide.

Interestingly, such interaction can lead to complete dissociation of the carbon monoxide molecule, as shown by isotope scrambling experiments on Rh(111).(26) By exposing an alkali predosed surface to two carbon monoxide labeled isotopes ($C^{13}O^{16}$ and $C^{12}O^{18}$), and looking

for the scrambling of these two in the thermal desorption products ($C^{13}O^{18}$, amu = 31), one can prove that carbon monoxide dissociation occurs. This happens of course only in the presence of a potassium adlayer. In the absence of such a layer, carbon monoxide does not dissociate on this clean transition metal surface at low pressures. Figure 30 shows the number of carbon monoxide molecules that dissociate per potassium atom. This number can reach a value greater than two at low potassium coverages.

7. Temperature Dependent Changes of Bonding of Adsorbed Molecules on Solid Surfaces

When an organic molecule is adsorbed on a transition metal surface and then heated, sequential dehydrogenation instead of desorption is observed. This is shown in Figure 31. From alkenes, hydrogen evolution is observed sequentially at well defined temperatures indicating that organic fragments are left behind on a transition metal surface. These organic fragments have been studied by a variety of techniques, the most powerful of which appears to be high resolution electron energy loss spectroscopy. Figure 32 shows the fragments that have been identified so far. There are CH, C_2, CH_2, and C_2H fragments that are all detectable. It appears that while these fragments would be free radical like in the gas phase, due to the strong metal carbon interaction, these are highly stable and well characterizable in well-defined temperature ranges on surfaces.(18) Only at the highest temperature of heat treatment does all the hydrogen release and the surface carbon graphitize to reach the thermodynamic end product of such a metal - organic molecule interaction.

Thus, there is sequential bond-breaking in adsorbed species which leads to the formation of surface intermediates that may be metastable in the thermodynamic sense. However, they are very stable in a well defined

temperature range. In fact, one can adsorb on a transition metal surface any number of very reactive organic molecules, and if the temperature is low enough, there is no chemical reaction. As the temperature in increased, there is sequential bond breaking and a CH, CC, CO, or CN bond will break leaving a fragment which is stable in a finite temperature range. Beyond this temperature, again, another bond breaking process occurs and again another fragment is left on the surface. Only at the very highest temperature will thermodynamically stable species form in the case of organic adsorbates. This stable state is a graphitized surface and hydrogen in the gas phase.

8. Adsorption and Chemical Bonding on High-Miller-Index, Stepped and Kinked Surfaces

Figure 33 shows the surface structures of several stepped surfaces of high Miller index. These surfaces are stable in a stepped/terrace configuration.(26) On the clean surface of a close-packed metal, the steps are usually of one atom in height, periodically distributed, and are separated by terraces of roughly equal width. Typical diffraction patterns of such surfaces are shown in Figure 34. The formation of doublets or triplets indicates the appearance of new periodicities from which the stepped structure of these high-Miller-index surfaces can be obtained.

When atoms or molecules adsorb on these high-Miller-index surfaces, they have available to them now several additional sites where their binding could be different. This is clearly indicated by thermal desorption spectroscopy studies. Figure 35 shows that carbon monoxide exhibits two desorption peaks at high coverages while at low coverages only the higher temperature desorption peak is present. The two desorption peaks, when compared with flat surfaces, can be attributed to carbon monoxide adsorbed

at stepped sites as well as the terrace sites. Since the adsorbed molecules at stepped sites desorb at the higher temperature, their binding is stronger than that at the terrace sites.

Figure 36 shows the desorption peaks of hydrogen after adsorption on flat, stepped and kinked platinum surfaces. On the kinked sites there are three desorption peaks. On the stepped sites there are two and on the flat surfaces there is only one. These desorption spectra make it relatively easy to associate the highest temperature desorption peak with hydrogen atoms at kinked sites, the middle one with hydrogen atoms at stepped sites, and the lowest temperature desorption peak with hydrogen atoms on terrace sites.

The surface chemical bond is highly structure sensitive. This is the major conclusion of studies of single crystal surfaces with adsorbates. Thus, if one measures the heat of adsorption as a function of atomic (Z) number across a transition metal series, one finds a diversity and richness of chemical bonding that is exhibited in Figure 37. Clearly, on each surface there may be many binding sites where the adsorbate is bound with different binding energies. There is no such thing as one adsorbate-substrate chemical bond. There may be four or five different bonding geometries with different heats of adsorption for a given atom or molecule on a given surface. This is one of the major reasons for the richness and diversity of surface chemistry that is exhibited in heterogeneous catalysis.

One should not give the impression that the stepped surfaces remain stable under all conditions. As Figure 38 shows, when surfaces are heated to higher temperature in the presence of certain adsorbates, they may undergo rearrangements which increase the the terrace width as well as

the step height, and which may ultimately lead to faceting.(27) Many of these changes may be reversible; many of them may not. The stability of surface structures is one of the major areas of surface science, since many surface chemical properties depend on surface structure stability.

9. The Effect of Surface Structure in Heterogeneous Catalysis

Surface structure sensitivity is well-illustrated by example from the field of catalysis. Figure 39 shows the rate of formation of ammonia from nitrogen and hydrogen on iron single crystal surfaces.(28) The open (111) crystal face is about 500 times more active in ammonia production than the close-packed (110) crystal face. In this reaction the dissociation of dinitrogen to nitrogen atoms is a rate-determining step. On the (111) surface there are sites where this dissociation process can occur with near zero activation energy. In these dissociation reactions, atoms at high coordination sites, which are found in the second layer near the surface, are implicated as the sites for bond-breaking. A more open surface makes the second layer high coordination metal atoms accessible to the incoming adsorbates, and this is one reason for the great reactivity of these more open surfaces.

The importance of surface structure in reactions can be shown by another example, ie. the hydrogen-deuterium exchange using mixed molecular beams of these two isotopes.(29) Figure 40 shows the scheme of the experiments. An incoming mixed molecular beam of hydrogen and deuterium is incident on a single crystal surface, and the product distribution is monitored as a function of angle with a mass spectrometer. By chopping the scattered beam, the velocity of the scattered beam can also be determined.

Figure 41 shows the reaction probability of forming HD from H_2 and D_2 on a stepped surface when the mixed beam hits the open side of the steps so that the fraction of atoms at the bottom of the step exposed is almost unity. As the beam changes direction so that the bottom of the steps are no longer exposed but are shielded, the reaction probability drops by a factor of 2. On the (111) surface where there are no steps the reaction probability is again down by about an order of magnitude. Clearly, in this case, H-H bond breaking occurs and this process is also highly structure sensitive.

10. Application of Modern Surface Science Techniques to Study the Solid-Liquid Interface

Recently a new technology was developed in our laboratory which is now applied widely in a large number of research groups that combines ultra-high vacuum surface science with high pressure catalytic reaction studies.(30) The cell that is used for this purpose is shown in Figure 42. The surface which is first exposed to ultra-high vacuum and characterized to determine the surface structure and surface composition is then isolated by an isolation cell which can be pressurized to several atmospheres to carry out a reaction study. Then the cell can be pumped, evacuated and opened, and the sample is sitting again in ultra-high vacuum where surface science studies can determine changes of surface structure and composition caused by the high pressure catalytic reaction.

Such a cell is also applicable for studies of reactions at solid-liquid interfaces that are important in electrochemistry and in colloid chemistry. In electrochemistry, several cells that can be filled with

liquids to study electrode reactions have been reported.(31) After electrochemical studies, the liquid is removed and the electrode is studied by modern surface science techniques.

We believe this approach will go a long way in allowing a molecular scrutiny of the solid-liquid interfaces that are present in colloid systems. We believe this is an important direction for surface science that will be of great asset to colloid scientists and those scientists interested in the molecular ingredients of systems and reactions at the solid-liquid interface.

ACKNOWLEDGEMENTS

This work was supported by the Director, Office of Energy Research, Office of Basic Energy Sciences, Chemical and Materials Sciences Division of the U.S. Department of Energy under Contract Number DE-AC03-76SF00098.

FIGURE CAPTIONS

Figure 1: Small surface area sample mounted in an ultra-high vacuum chamber prepared for surface studies.

Figure 2: Experimental number of scattered electrons, n(E), of energy, E, versus electron energy for a Rh(111) surface covered with a monolayer of ethylidyne species (CCH_3) species--the stable, room temperature structure of chemisorbed ethylene. Boxes and inset figures show how particular scattered electrons are used in (a) Auger electron spectroscopy, (b) high resolution electron energy loss spectroscopy and (c) low energy electron diffraction.

Figure 3: Typical Auger spectra from pure Au, two alloys, and pure Ag.

Figure 4: Surface excess of silver as a function of bulk composition in silver-gold alloys.

Figure 5: The ideal and regular solid solution models that predict surface segregations of the constituents with lower surface free energy.

Figure 6: Model of a heterogeneous solid surface, depicting different surface sites. These sites are distinguishable by their number of nearest neighbors.

Figure 7: Idealized atomic surface structures for the flat Pt(111) and Pt(100), the stepped Pt(755), and the kinked Pt(10,8,7) surfaces.

Figure 8:
a) Diffraction pattern from the Pt(100) 5x1 structure.
b) Schematic representation of the 100 surface with hexagonal overlayer.
c) Diffraction pattern from the Pt(100) 1x1 structure.
d) Schematic representation of the 100 surface.

Figure 9: Structure of the reconstructed Pt(100) crystal face as solved by surface crystallography.

Figure 10: Top and side views of ideal, bulk-like Si(100) at the left and Si(100) p(2x1) in the modified Schlier-Farnsworth model at the right. Layer-spacing contractions and intralayer atomic displacement relative to the bulk structure are given. Shading differentiates surface layers.

Figure 11: Low-energy electron diffraction patterns taken at four different energies of the reconstructed Si(111) crystal face exhibiting a (7x7) surface structure.

Figure 12: Top and side views (in top and bottom sketches of each panel) of adsorption geometries on various metal surfaces. Adsorbates are drawn shaded. Dotted lines represent clean surface atomic positions; arrows show atomic displacements due to adsorption.

Figure 13: Scheme of building catalyst monolayers of well-characterized structural composition. Metal atoms are condensed from the vapor phase on single-crystal metal surfaces until desired amounts and atomic structures are obtained.

Figure 14: (left) Comparison of adsorption bond lengths at surfaces (arrows show uncertainty) with equivalent bond lengths in molecules and bulk compounds (blocks extending over range of values found in standard tables). (right) Induced charge transfers for adsorption as determined by work function change, distance of adsorbate from the surface, and surface charge and dipolar charge density.

Figure 15: Thermal desorption spectra of carbon monoxide on Rh(111) measured as a function of coverage following adsorption near 300 K. The crystal heating rate was linear at 15K/sec. Note the desorption peak temperature shift as a function of coverage.

Figure 16: Isosteric heat of adsorption for CO on the Pd(111) crystal face as a function of coverage. (After H. Conrad, G. Ertl, J. Koch, and E.E. Latta, Surf. Sci. 43, 462 [1974]).

Figure 17: Top site bonding structure of carbon monoxide on Ni(100) from low energy electron diffraction and electron spectroscopy studies.

Figure 18: Bridge site adsorption structure of carbon monoxide on Pd(100) at a half monolayer coverage.

Figure 19: Structure determined by low energy electron diffraction for a saturation coverage of carbon monoxide on Rh(111). Top and side views are shown. Large circles represent Rh atoms while smaller circles correspond to C and O atoms. Solid lines show the structure expected for hexagonal close-packing of the carbon monoxide while dotted circles depict the actual structure.

Figure 20: The two-dimensional phase approximation. Potential energy barriers for desorption or bulk diffusion are much larger than for surface diffusion, so equilibrium is attained in two dimensions only.

Figure 21: The surface structure of ethylidyne (bond distances and angles) is compared with several tri-nuclear metal cluster compounds of similar structure.

Figure 22: High resolution electron energy loss vibrational spectrum of ethylidyne (CCH_3) and ethylidyne-d_3 on Rh(111): the stable, room temperature, chemisorbed structure for ethylene.

Figure 23: Surface structures for alkylidyne species formed on Pt(111) after the adsorption and rearrangement of ethylene, propylene, and butenes. These structures were determined by surface crystallography and high resolution electron energy loss spectroscopy.

Figure 24: Surface structure of benzene as determined from low energy electron diffraction studies and surface crystallography.

Figure 25: The vibrational spectra of benzene and deuterated benzene adsorbed on a Rh(111) surface as determined by high resolution electron energy loss spectroscopy.

Figure 26: Monolayer and multilayer surface phases of the n-paraffins C_3-C_8 on Pt(111) and the temperatures at which they are observed at 10^{-7} torr.

Figure 27: The site-blocking effect of sulfur on deuterium adsorption on Mo(100) as determined by deuterium thermal desorption. (o) = sulfur layer disordered, (x) = sulfur layer ordered. The broken line is a theoretical prediction of the site-blocking effect assuming that one sulfur atom blocks one deuterium atom adsorption site and that deuterium molecules chemisorb dissociatively in adjacent, unoccupied sites.

Figure 28: Vibrational spectra of the saturation carbon monoxide coverage chemisorbed on Pt(111) at 300K as a function of preadsorbed potassium coverage.

Figure 29: Interaction of gas phase carbon monoxide molecular orbitals with the filled energy levels of a transition metal to form bonding orbitals for associatively adsorbed CO.

Figure 30: Carbon monoxide dissociation on a Rh(111) surface as a function of potassium coverage as determined by thermal desorption isotope scrambling experiments with $C^{13}O^{16}$ and $C^{12}O^{18}$.

Figure 31: Hydrogen thermal desorption spectra illustrating the sequential dehydrogenation of ethylene, propylene, and cis-2-butene chemisorbed on the Pt(111) crystal surface at 120K. The rate of heating is 12 K/sec.

Figure 32: Schematic representation of the various organic fragments that are present on metal surfaces at higher temperature. The presence of CH, C_2, C_2H, CH_2, and CCH_3 species has been detected.

Figure 33: Structure of several high-Miller-index stepped surfaces with different terrace widths and step orientations.

Figure 34: Low energy electron diffraction patterns of the (a) Pt(755), (b) Pt(679), (c) Pt(544), and (d)Pt(533) stepped surfaces.

Figure 35: Thermal desorption spectra of carbon monoxide from a Pt(533), stepped crystal face as a function of coverage. The two peaks are indicative of CO bonding at step and terrace sites. The higher temperature peak corresponds to CO bound at step sites.

Figure 36: Thermal desorption spectra for hydrogen chemisorbed on flat Pt(111), stepped Pt(557), and kinked Pt(12,9,8) surfaces.

Figure 37: Heats of adsorption of carbon monoxide on single crystal surfaces of transition metals.

Figure 38: Schematic representation of surfaces exhibiting one-atom step height configuration, multiple-height step structure, and hill-and-valley configuration consisting of large facet planes. Reconstruction from on type to another may occur on adsorption and/or heating.

Figure 39: The remarkable surface structure sensitivity of the iron-catalyzed, ammonia synthesis.

Figure 40: Scheme of the molecular beam - surface scattering experiment.

Figure 41: HD production as a function of angle of incidence, θ , of the molecular beam, normalized to the incident D_2 intensity. (a) Pt(332) with step edges perpendicular to the incident beam (Φ=90°); (b) Pt(332) where the projection of the beam on the surface is parallel to the step edges (Φ=0°); (c) Pt(111).

Figure 42: Schematic representation of the experimental apparatus to carry out catalytic-reaction-rate studies on single crystal surfaces of low surface area at low and high pressures in the range of 10^{-7} to 10^{4} torr.

REFERENCES

1. G.A. Somorjai, Chemistry in Two Dimensions: Surfaces, Cornell University Press, 1981.

2. G. Ertl and J. Küppers, Low Energy Electrons and Surface Chemistry, Verlag Chemie, Weinheim, 1979.

3. M.A. Van Hove and S.Y. Tong, Surface Crystallography by Low-Energy Electron Diffraction: Theory, Computation and Structural Results, Springer-Verlag, Heidelberg, 1979.

4. H. Ibach and D.L. Mills, Electron Energy Loss Spectroscopy and Surface Vibrations, Academic Press, New York, 1982.

5. B. Feuerbacher, B. Fitton, and R.F. Willis, eds., Photoemission and the Electronic Properties of Surfaces, Wiley, London, 1979.

6. C.C. Chang, "Analytical Auger Electron Spectroscopy" in Characterzation of Solid Surfaces, P.F. Kane and G.B. Larrabee, eds., Plenum Press, New York, 1974.

7. A. Jablonski, S.H. Overbury and G.A. Somorjai, Surf. Sci. 65, 578 (1977).

8. S. Overbury, P. Bertrand and G.A. Somorjai, Chem. Rev. 75 (5), 550 (1975).

9. S. Hagstrom, H.B. Lyon and G.A. Somorjai, Phys. Rev. Lett. 15, 491 (1965).

10. M.A. Van Hove, R.J. Koestner, P.C. Stair, J.P. Biberian, L.L. Kesmodel and G.A. Somorjai, Surf. Sci. 103, 189 (1981); Surf. Sci. 103, 218 (1981).

11. J. Appelbaum and D.R. Hamann, Surf. Sci. 74, 21 (1978); K.A.R. Mitchell and M.A. Van Hove, Surf. Sci. 75, 147L (1978); S.Y. Tong and A.L. Maldonado, Surf. Sci. 78, 459 (1978); J.A. Appelbaum, G.A. Baraff, and D.R. Hamann, Phys. Rev. Lett. 35,729 (1975); Phys. Rev. B14, 588 (1976).

12. J.W.A. Sachtler and G.A. Somorjai, Phys. Rev. Lett. 45, 1601 (1980).

13. P.A. Redhead, Vacuum 12, 203 (1962).

14. J.E. Crowell and G.A. Somorjai, Applied Surf. Sci., Submitted Nov. 1983.

15. S. Andersson and J.B. Pendry, Surf. Sci. 71, 75 (1978).

16. H.J. Behm, K. Christmann, G. Ertl, and M.A. Van Hove, Surf. Sci. 88, L59 (1979).

17. M.A. Van Hove, R.J. Koestner, J.C. Frost and G.A. Somorjai, Surf. Sci. 129(2/3), 482 (1983);

18. R.J. Koestner, M.A. Van Hove and G.A. Somorjai, J. Phys. Chem. 87, 203 (1983); Surf. Sci. 121 321 (1982).

19. L.H. Dubois, D.G. Castner and G.A. Somorjai, J. Chem. Phys. 72, 5234 (1980); H. Steininger, H. Ibach and S. Lehwald, Surf. Sci. 117, 685 (1980).

20. B.E. Koel, B.E. Bent and G.A. Somorjai, Surf. Sci., in Press 1984.

21. L.L. Kesmodel, L.H. Dubois and G.A. Somorjai, J. Chem. Phys. 70, 2180 (1979).

22. B.E. Koel, J.E. Crowell, C.M. Mate and G.A. Somorjai, J. Phys. Chem., In Press (1984).

23. L.E. Firment and G.A. Somorjai, J. Chem. Phys. 66(7), 2901 (1977).

24. M.H. Farias, A.J. Gellman, R.R. Chianelli, K.S. Liang and G.A. Somorjai, Surf. Sci. 140, 181 (1984).

25. J.E. Crowell, E.L. Garfunkel and G.A. Somorjai, Surf. Sci. 121, 303 (1982).

26. J.E. Crowell, W.T. Tysoe and G.A Somorjai (to be published).

27. D.W. Blakely and G.A. Somorjai, Surf. Sci. 65, 491 (1977).

28. N.D. Spencer, R.C. Schoonmaker and G.A. Somorjai, J. Catal. 74, 129 (1982); Nature 294, 643 (1981).

29. M. Salmeron, R.J. Gale and G.A. Somorjai, J. Chem. Phys. 70(06), 2807 (1979).

30. A.L. Cabrera, N.D. Spencer, E. Kozak, P.W. Davies and G.A. Somorjai, Rev. Sci. Instrum. 53, 1888 (1982); D.W. Blakely, E.I. Kozak, B.A. Sexton and G.A. Somorjai, J. Vac. Sci. Technol. 13, 1091 (1976).

31. A.T. Hubbard, Acc. Chem. Res., 13, 177 (1980); P.N. Ross, Jr. in Chemistry and Physics of Solid Surfaces IV, R. Vanselow and R. Howe, eds., Springer-Verlag, 1982.

TABLE I

Table of surface characterization techniques that are used to determine the structure and composition of solid surfaces. Adsorbed species present at concentrations of 1% of a monolayer can be readily detected.

SURFACE ANALYSIS METHOD	ACRONYM	PHYSICAL BASIS	TYPE OF INFORMATION OBTAINED
Low energy electron diffraction	LEED	Elastic backscattering low energy electrons	Atomic surface structure of surfaces and of adsorbed gases
Auger electron spectroscopy	AES	Electron emission from surface atoms excited by electron x-ray or ion bombardment	Surface composition
High resolution electron energy loss spectroscopy	HREELS	Vibrational excitation of surface atoms by inelastic reflection of low energy electrons	Structure and bonding of surface atoms and adsorbed species.
Infrared spectroscopy	IRS	Vibrational excitation of surface atoms by adsorption of infrared radiation.	Structure and bonding of adsorbed gases.
X-ray and ultraviolet photoelectron spectroscopy	XPS UPS	Electron emission from atoms	Electronic structure and oxidation state of surface atoms and adsorbed species.
Ion scattering spectroscopy	ISS	Inelastic reflection of inert gas ions.	Atomic structure and composition of solid surfaces
Secondary ion mass spectroscopy	SIMS	Ion beam induced ejection of surface atoms as positive & negative ions	Surface composition
Extended X-ray absorption fine structure analysis	EXAFS	Interference effects during x-ray emission	Atomic structure energetics composition of adsorbed species
Thermal desorption spectroscopy	TDS	Thermally induced desorption or decomposition of adsorbed species	Adsorption energetics composition of adsorbed species
Solid state nuclear magnetic resonance	Solid-state NMR	Nuclear magnetic resonance on samples with areas of 1 m2 or larger	Atomic and molecular composition, structure

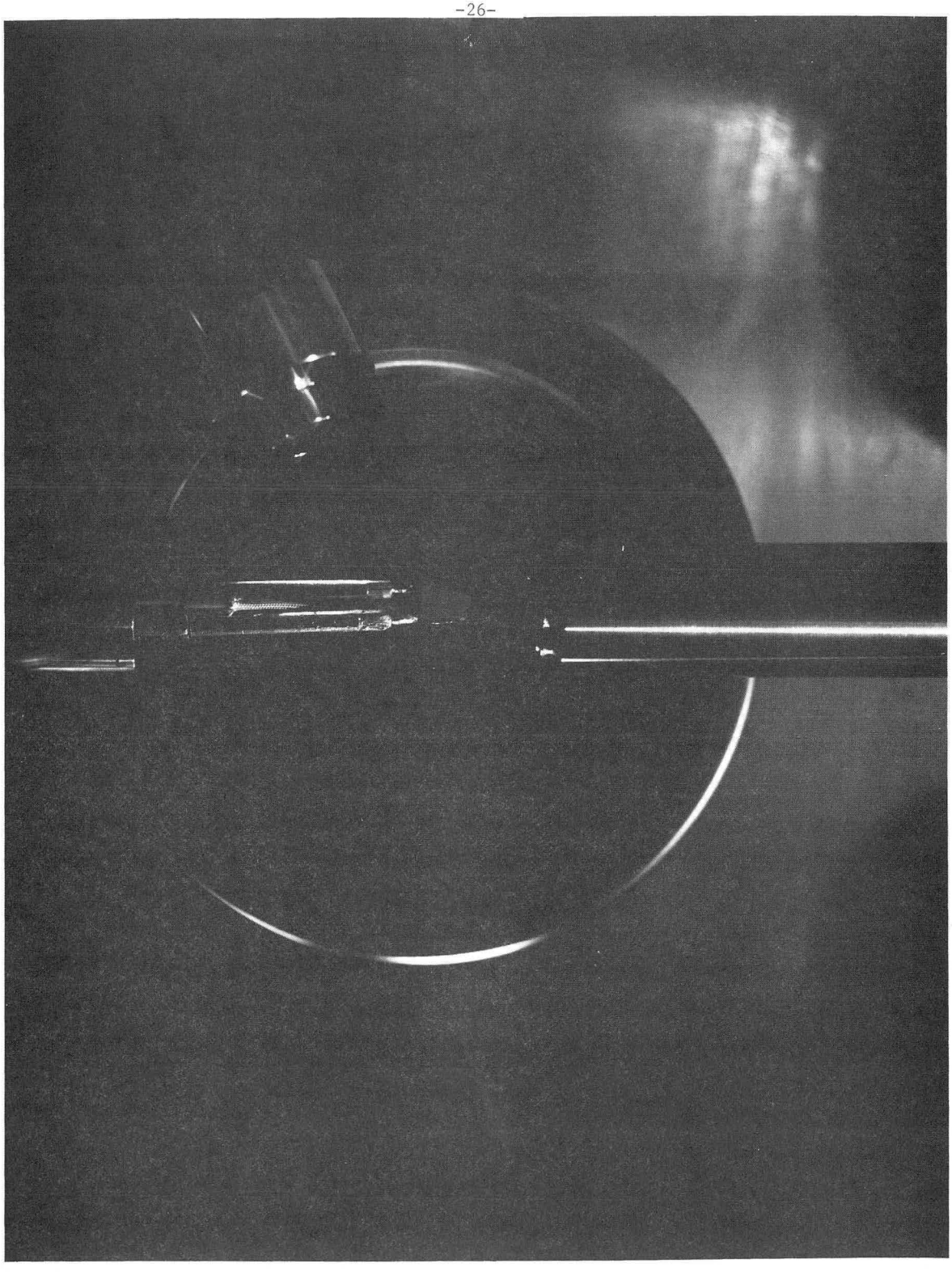

CBB 819-9186

Figure 1

ENERGY DISTRIBUTION OF SCATTERED ELECTRONS FROM A c(4×2) MONOLAYER OF C_2H_3 ON Rh(111) AT 300K

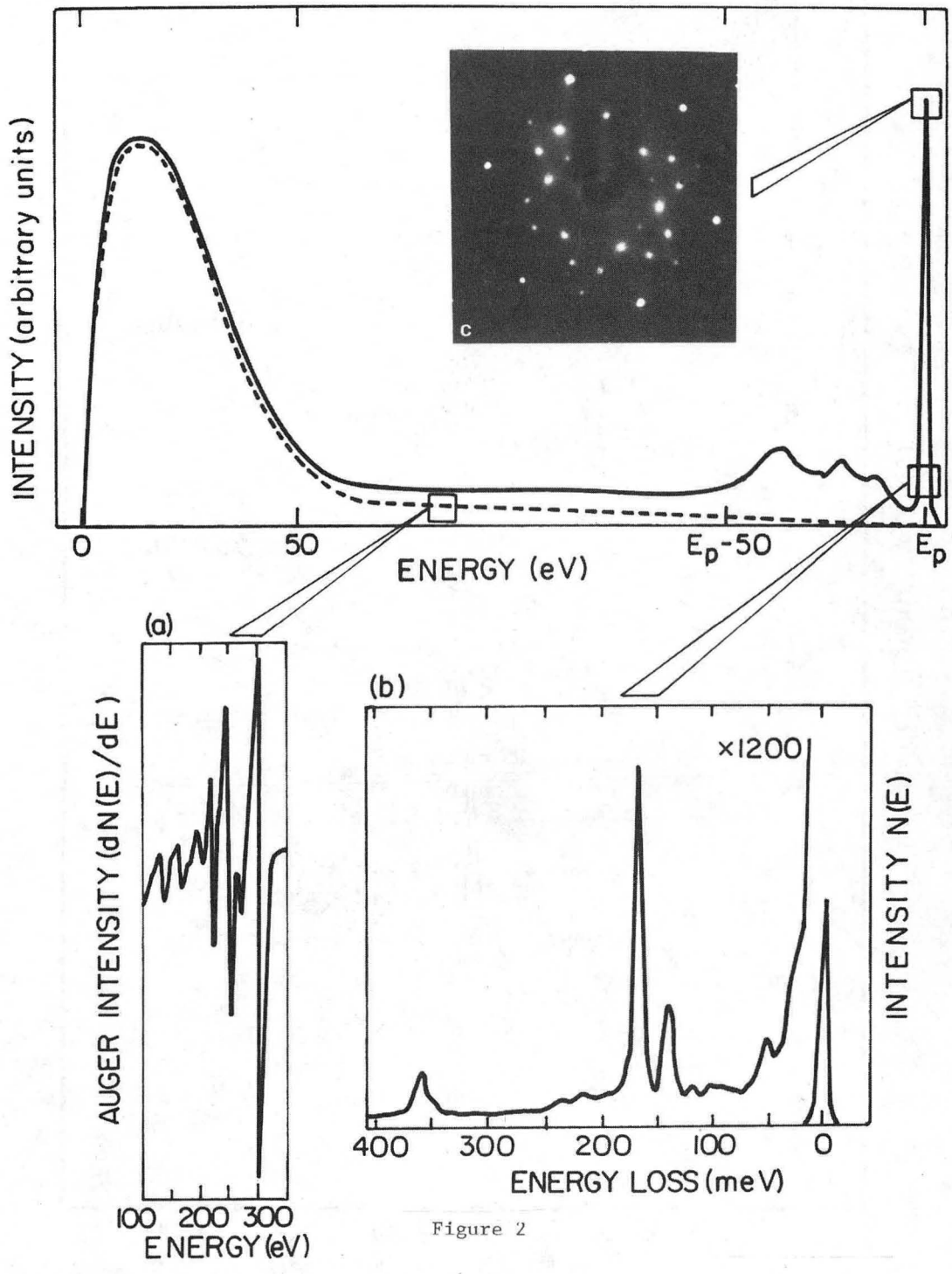

Figure 2

XBB 8312-11012

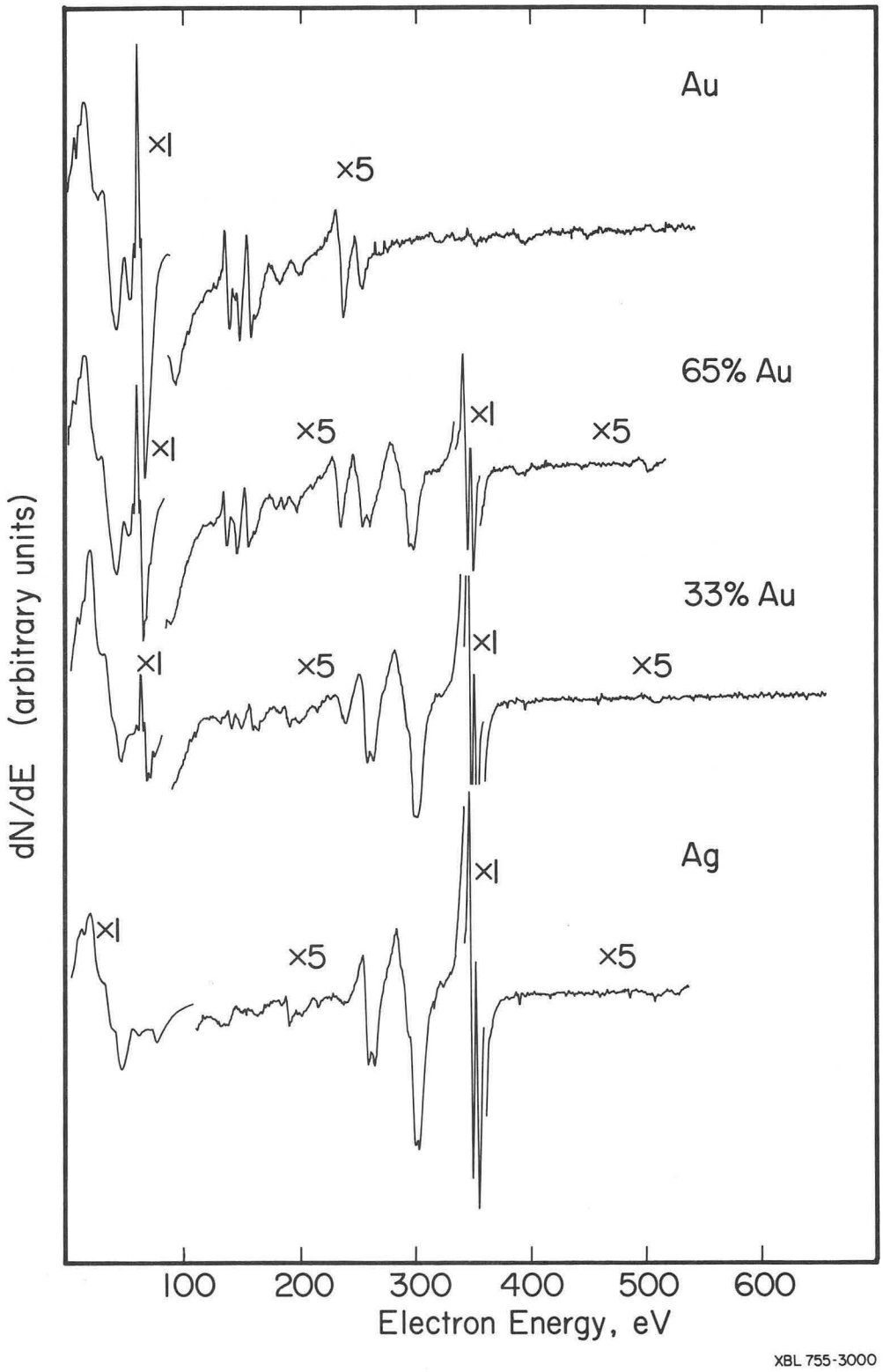
Au
×1
×5
65% Au
×1
×5
×1
×5
33% Au
×1
×5
×1
×5
Ag
×1
×5
×1
×5
dN/dE (arbitrary units)
100
200
300
400
500
600
Electron Energy, eV
XBL 755-3000

Figure 3

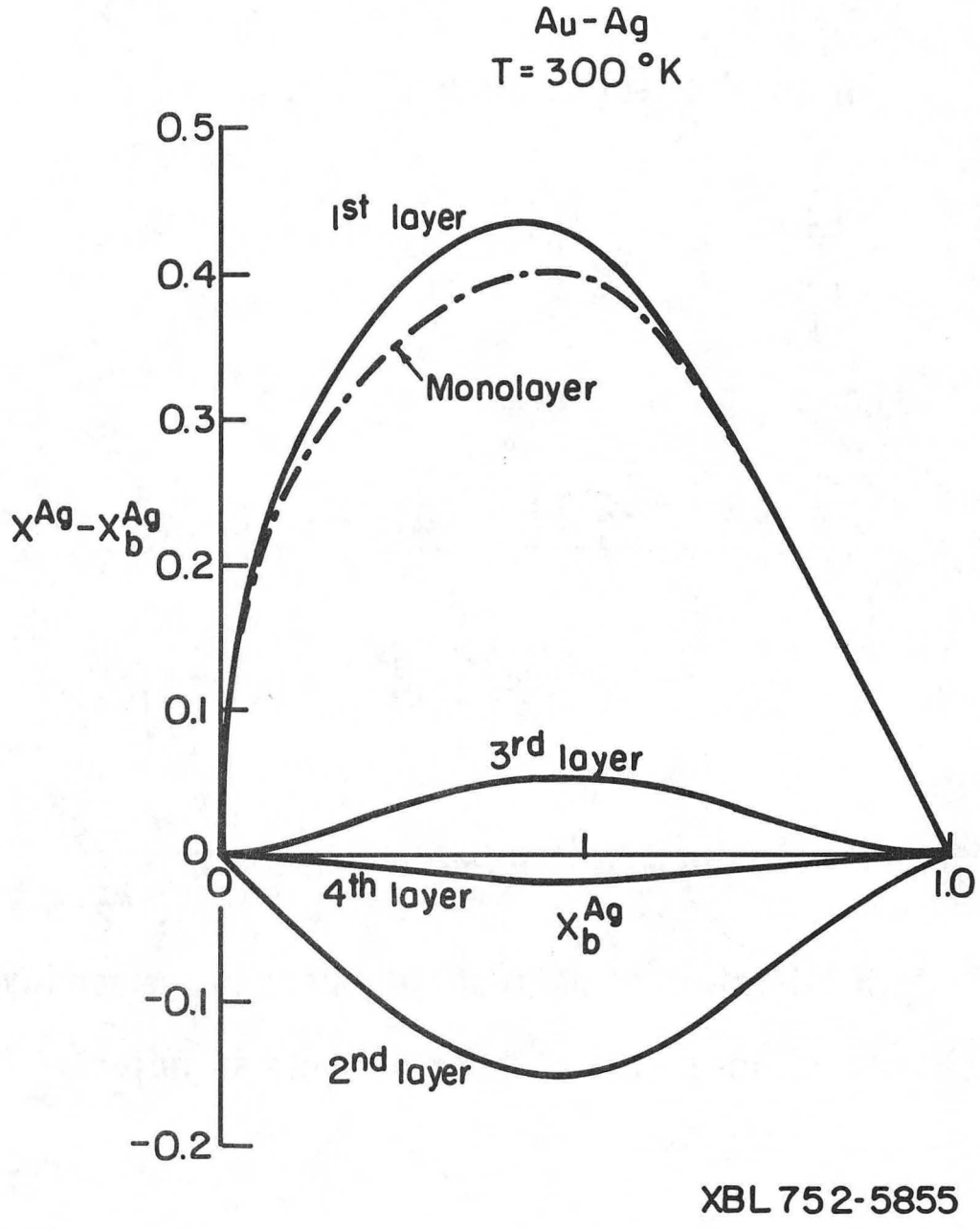
Au-Ag
T = 300 °K
0.5
0.4
0.3
0.2
0.1
0
-0.1
-0.2
$X^{Ag} - X_b^{Ag}$
1st layer
Monolayer
3rd layer
4th layer
2nd layer
0
1.0
X_b^{Ag}
XBL 752-5855

Figure 4

For an ideal solid solution:

$$\frac{x_2^s}{x_1^s} = \frac{x_2^b}{x_1^b} \exp\left[\frac{(\sigma_1 - \sigma_2)a}{RT}\right]$$

For a regular solid solution:

$$\frac{x_2^s}{x_1^s} = \frac{x_2^b}{x_1^b} \exp\left[\frac{(\sigma_1 - \sigma_2)a}{RT}\right] \exp\left\{\frac{\Omega(\ell + m)}{RT}\left[(x_1^b)^2 - (x_2^b)^2\right] - \frac{\Omega\ell}{RT}\left[(x_2^s)^2 - (x_1^s)^2\right]\right\}$$

where Ω = regular solution parameter = $\dfrac{\Delta H_{mixing}}{x_1^b \cdot x_2^b}$

ℓ = fraction of nearest neighbors in surface layer.

m = fraction of nearest neighbors in adjacent layer.

XBL 741-234

Figure 5

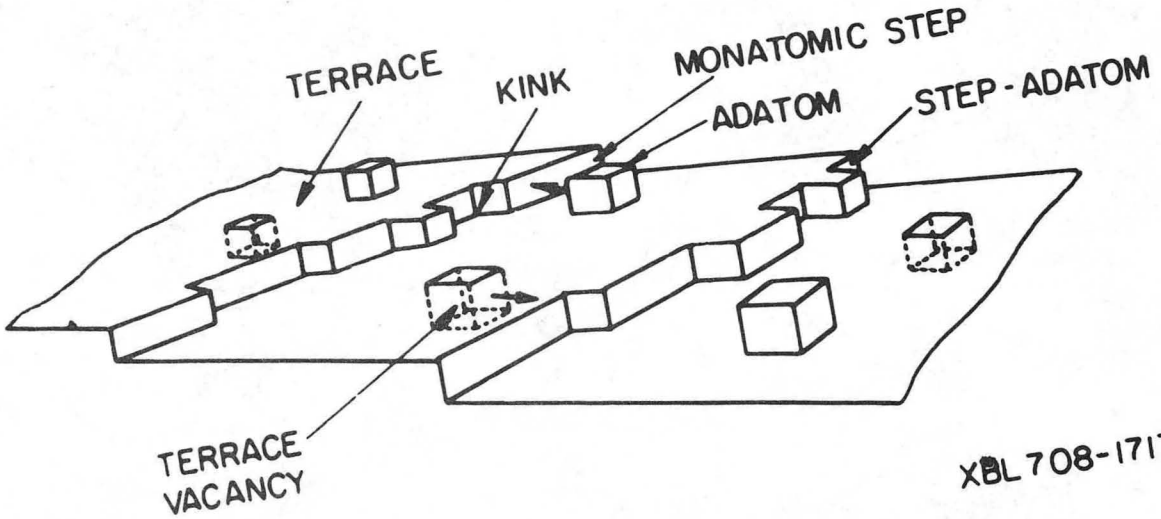
TERRACE
KINK
MONATOMIC STEP
ADATOM
STEP-ADATOM
TERRACE
VACANCY
XBL 708-1717A

Figure 6

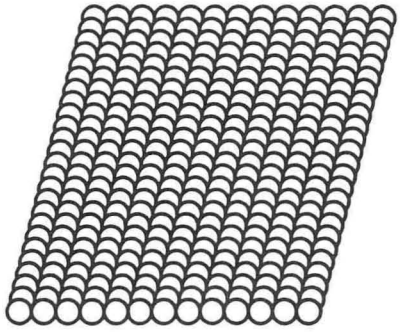

fcc (100)

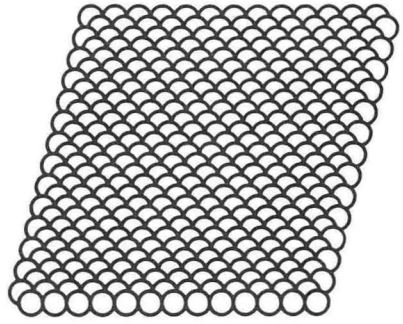

fcc (111)

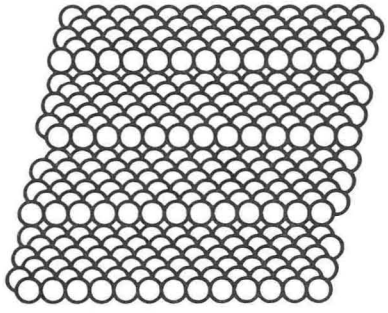

fcc (755)

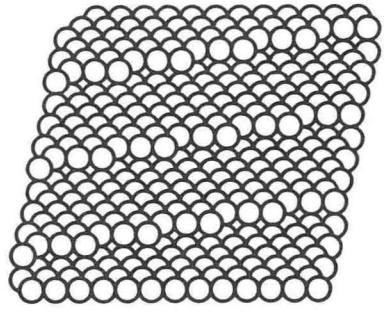

fcc (10.8.7)

XBL 8112-13009

Figure 7

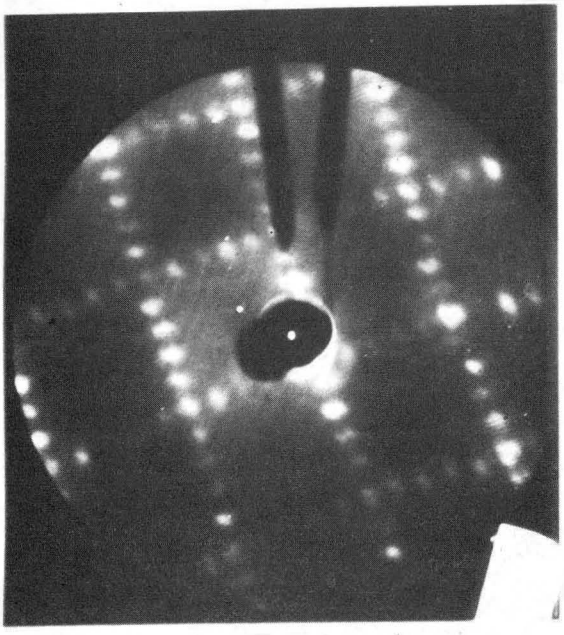

(a)

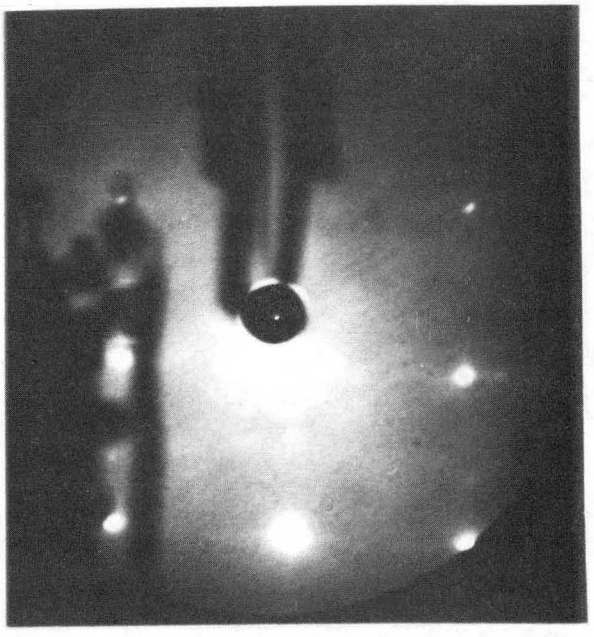

(c)

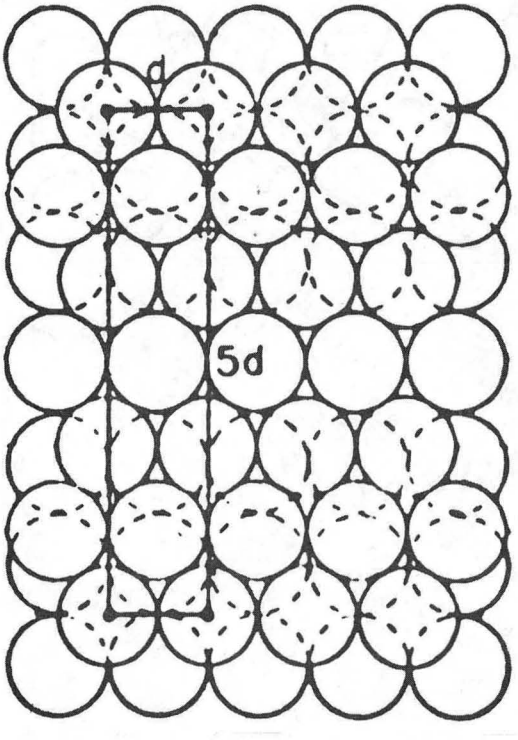

(b)

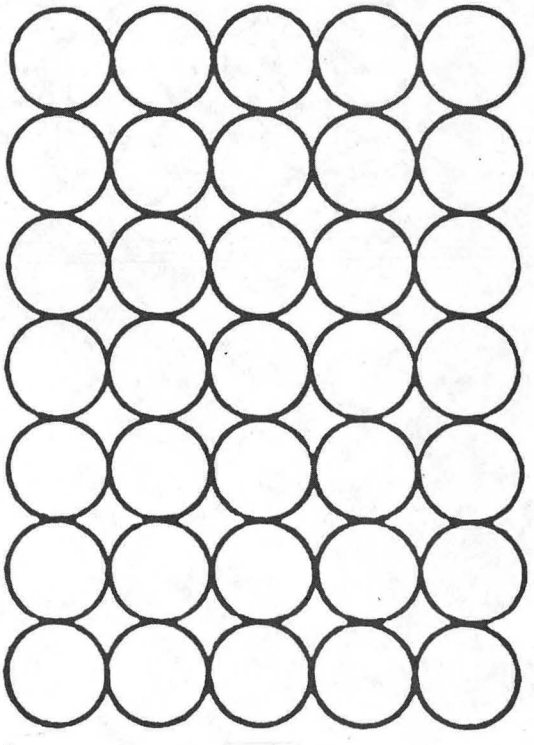

(d)

Figure 8

XBB 7111-5356

fcc (100) : buckled hexagonal top layer

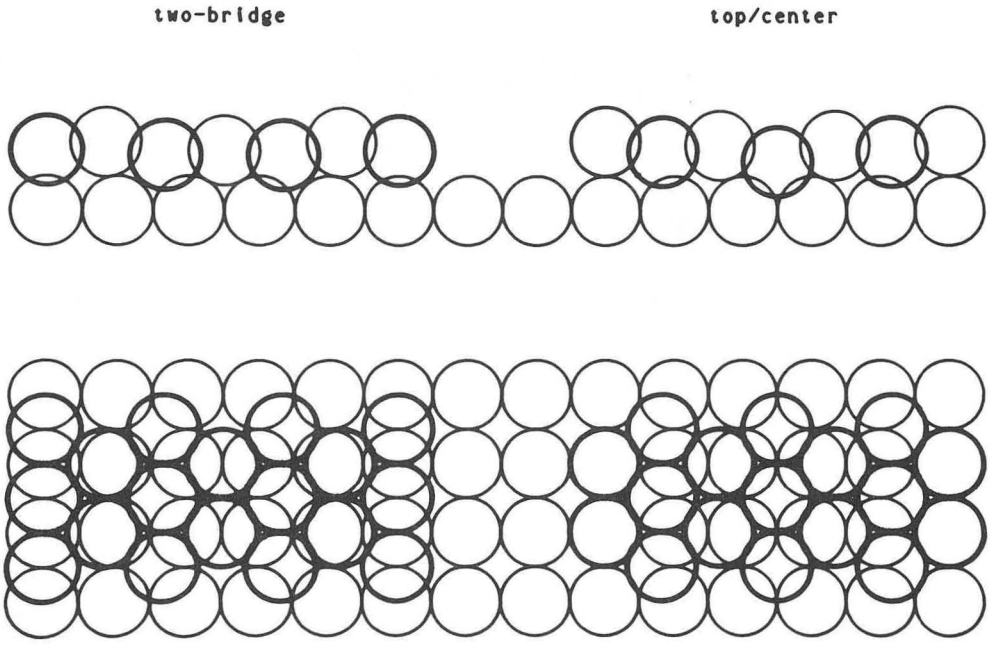

XBL 7912-13739

Figure 9

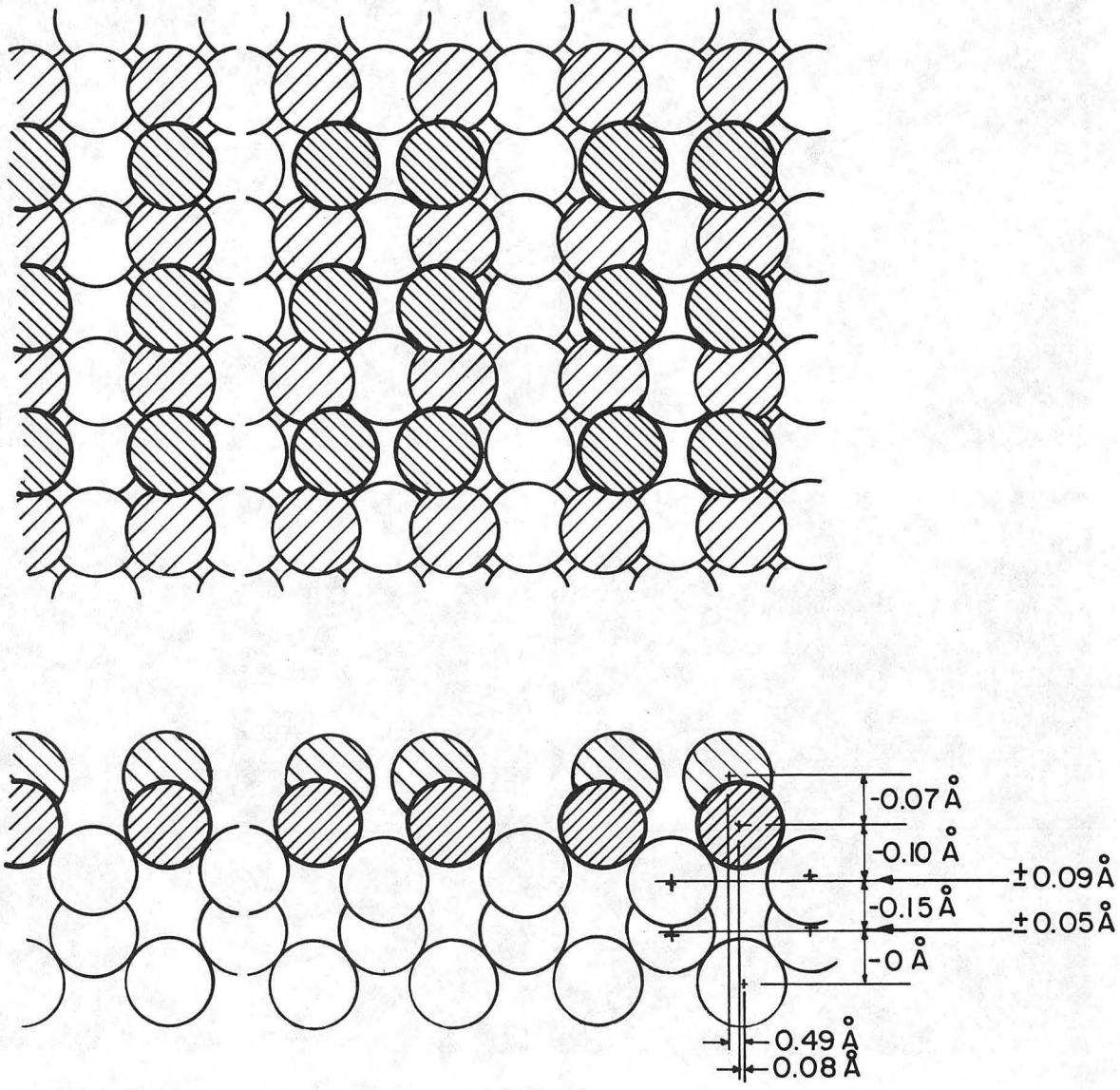
-0.07 Å
-0.10 Å
±0.09 Å
-0.15 Å
±0.05 Å
-0 Å
0.49 Å
0.08 Å
Si (100)
ideal
Si (100)
p(2x1)
XBL 7812-6285

Figure 10

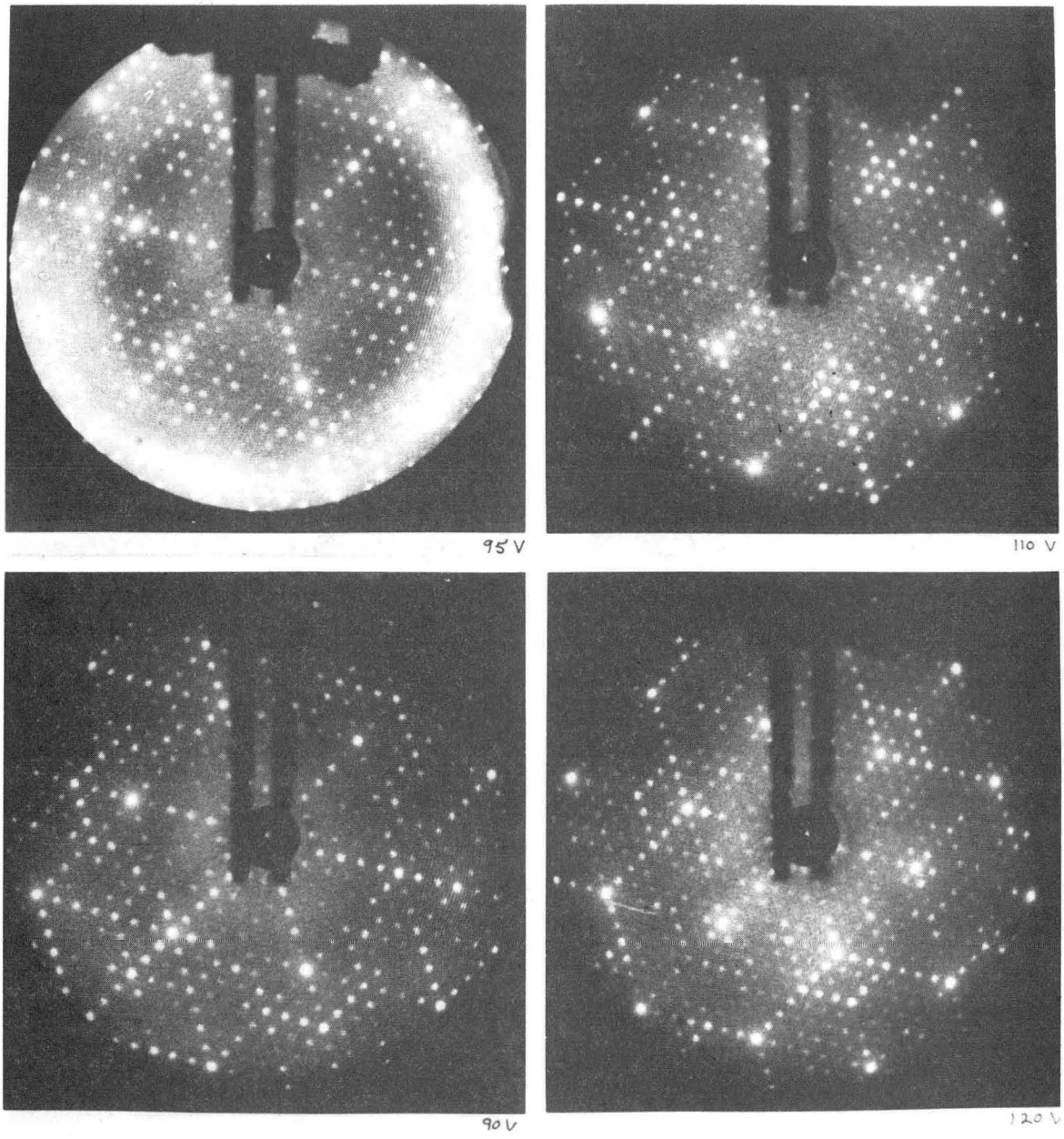

XBB 846-4625

Figure 11

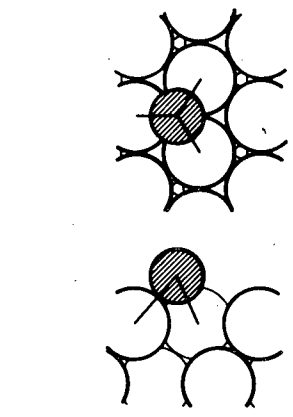

(a) fcc(111), hcp(0001): hollow site

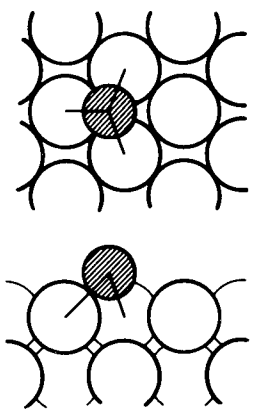

(b) bcc(110): 3-fold site

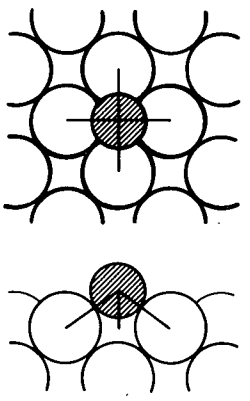

(c) fcc(100): hollow site

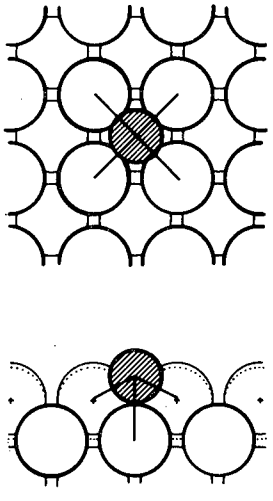

(d) bcc(100): hollow site

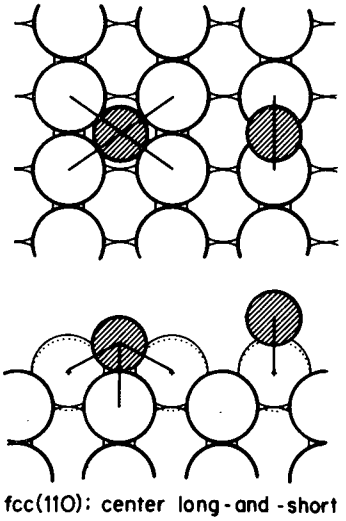

(e) fcc(110): center long-and-short bridge sites

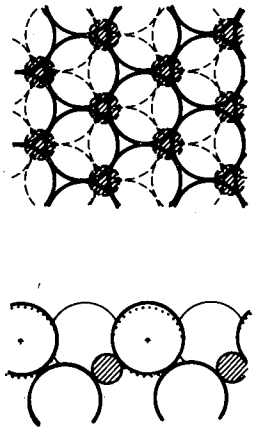

(f) hcp (0001): underlayer

XBL 7812-6293

Figure 12

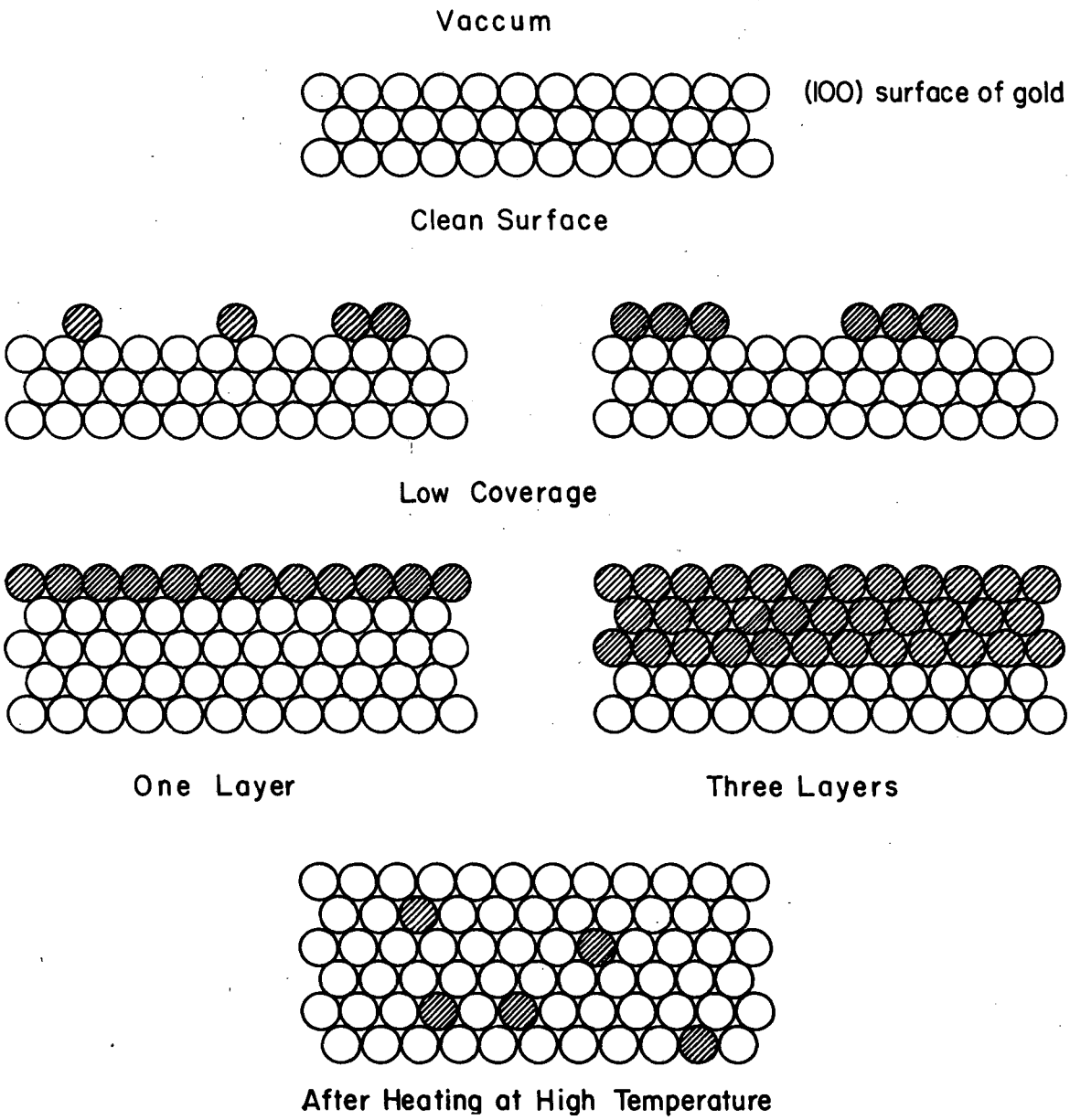
Vaccum
(100) surface of gold
Clean Surface
Low Coverage
One Layer
Three Layers
After Heating at High Temperature
XBL 7810-6070

Figure 13

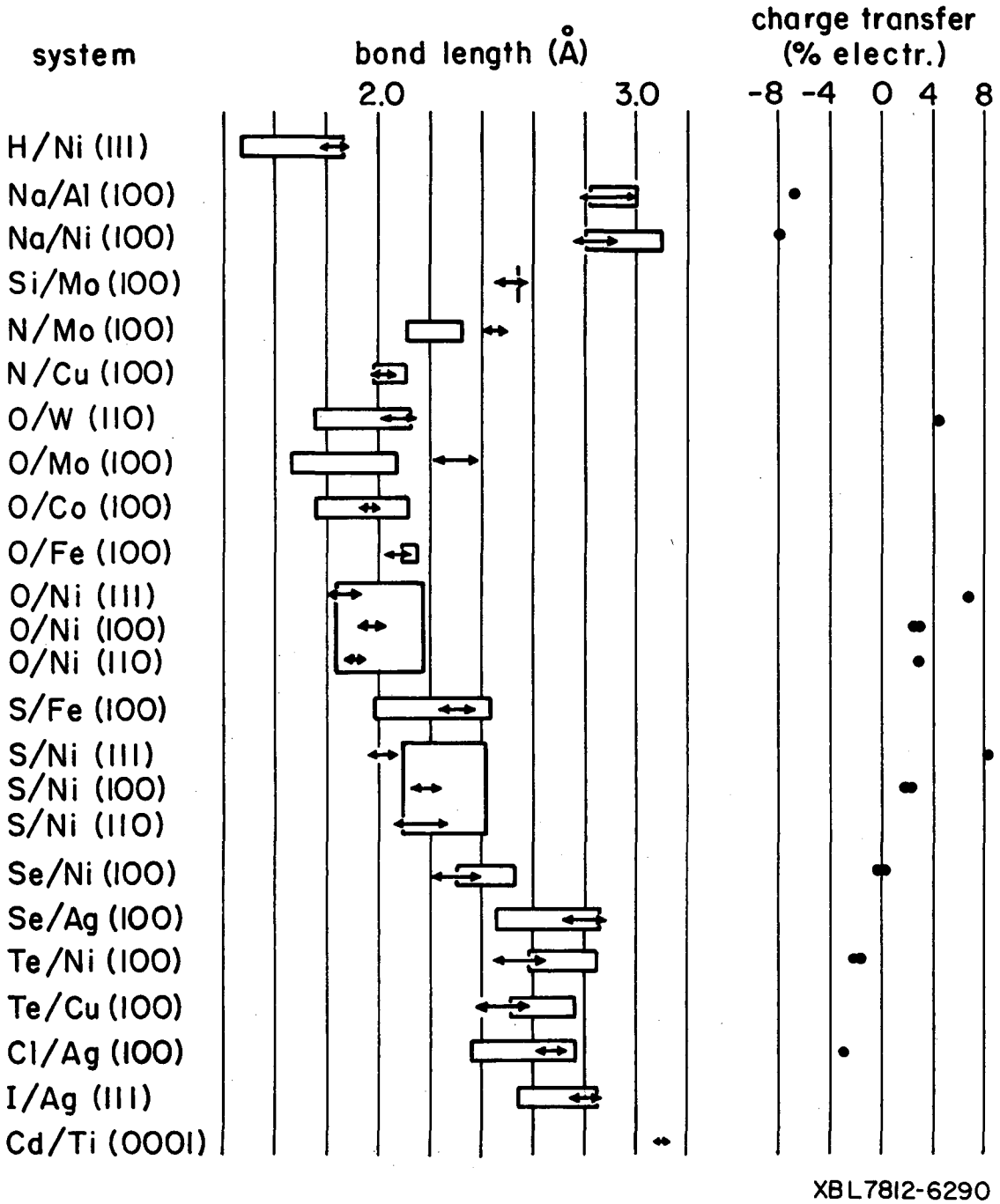
system
bond length (Å)
2.0
3.0
charge transfer
(% electr.)
-8 -4 0 4 8
H/Ni (111)
Na/Al (100)
Na/Ni (100)
Si/Mo (100)
N/Mo (100)
N/Cu (100)
O/W (110)
O/Mo (100)
O/Co (100)
O/Fe (100)
O/Ni (111)
O/Ni (100)
O/Ni (110)
S/Fe (100)
S/Ni (111)
S/Ni (100)
S/Ni (110)
Se/Ni (100)
Se/Ag (100)
Te/Ni (100)
Te/Cu (100)
Cl/Ag (100)
I/Ag (111)
Cd/Ti (0001)
XBL7812-6290

Figure 14

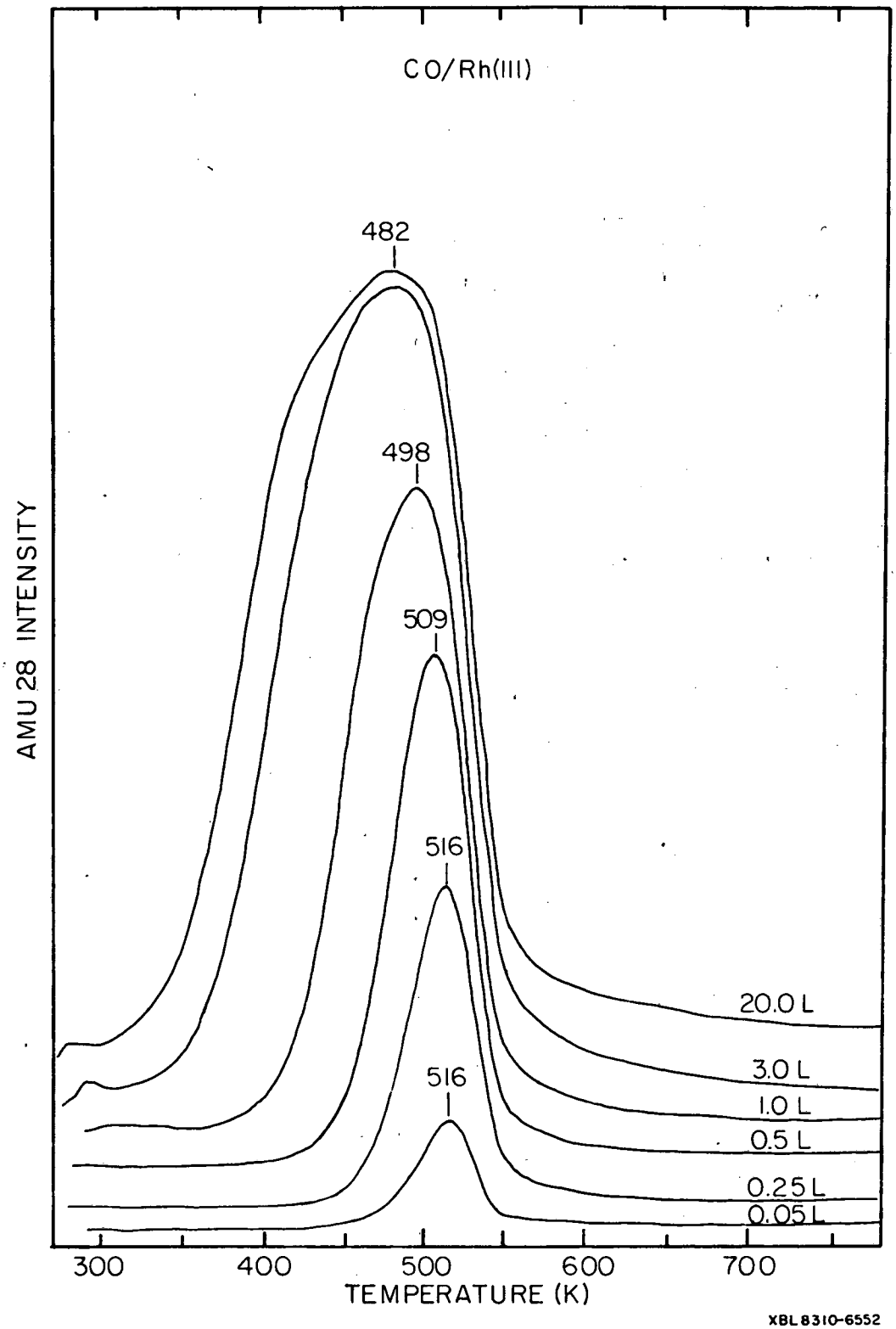
CO/Rh(111)
482
498
509
516
516
20.0 L
3.0 L
1.0 L
0.5 L
0.25 L
0.05 L
AMU 28 INTENSITY
300
400
500
600
700
TEMPERATURE (K)
XBL 8310-6552

Figure 15

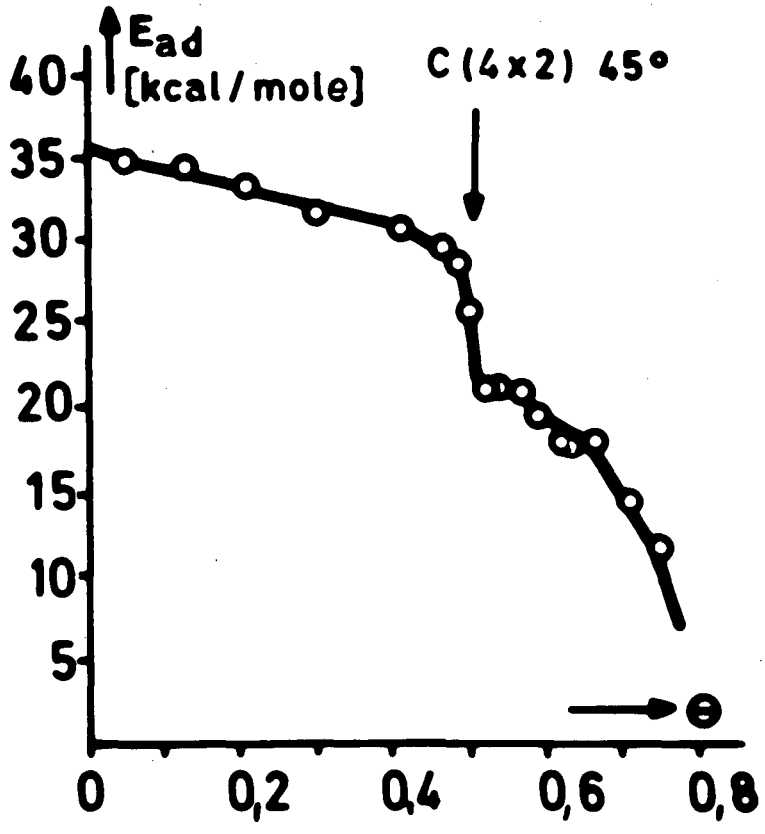

XBL 7911-12823

Figure 16

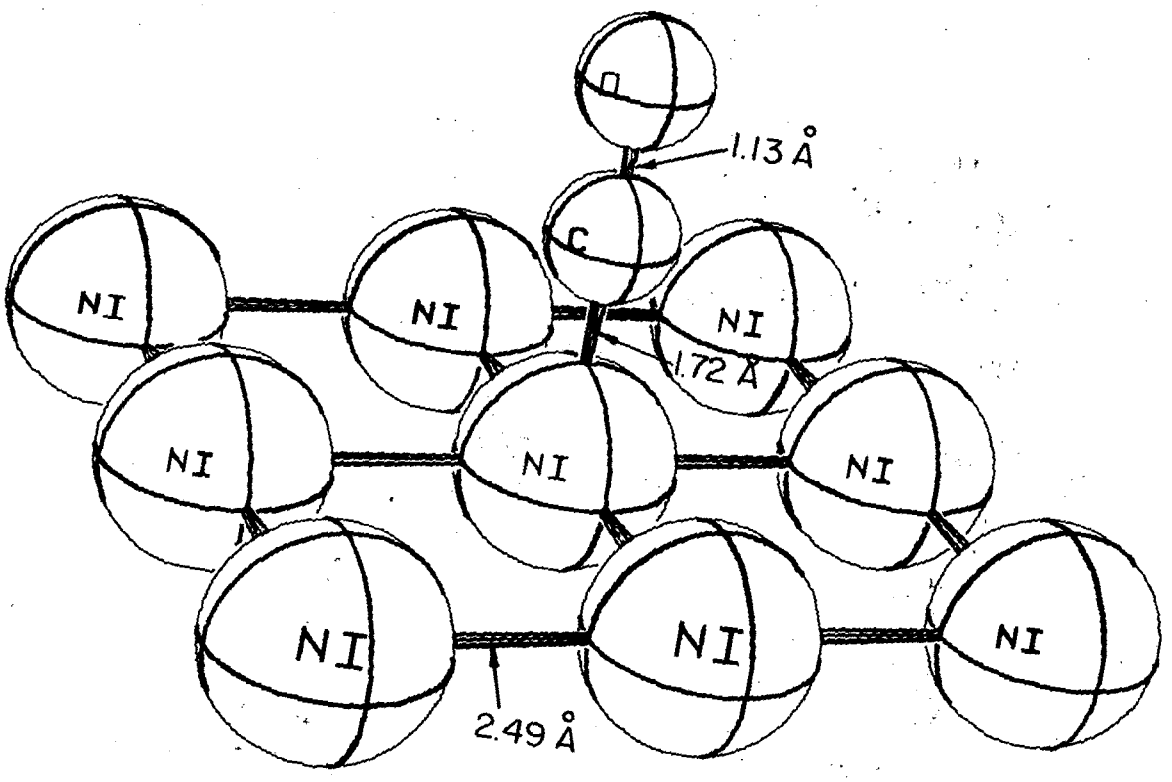

Ni (100) + c (2x2) CO

XBL 794-6169

Figure 17

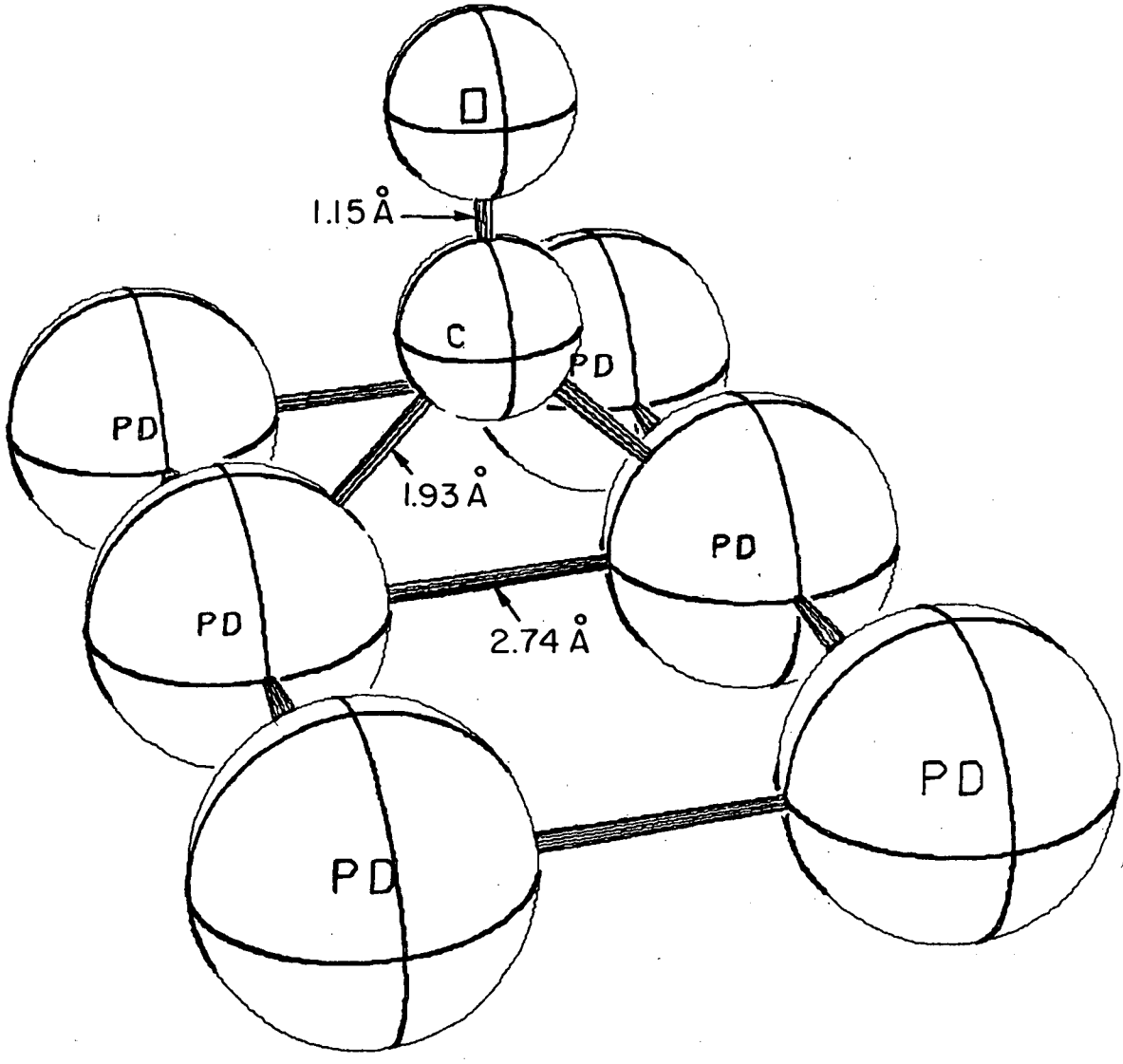

Pd (100) + $(2\sqrt{2}\times\sqrt{2})$ R 45° 2 CO

XBL794-6170

Figure 18

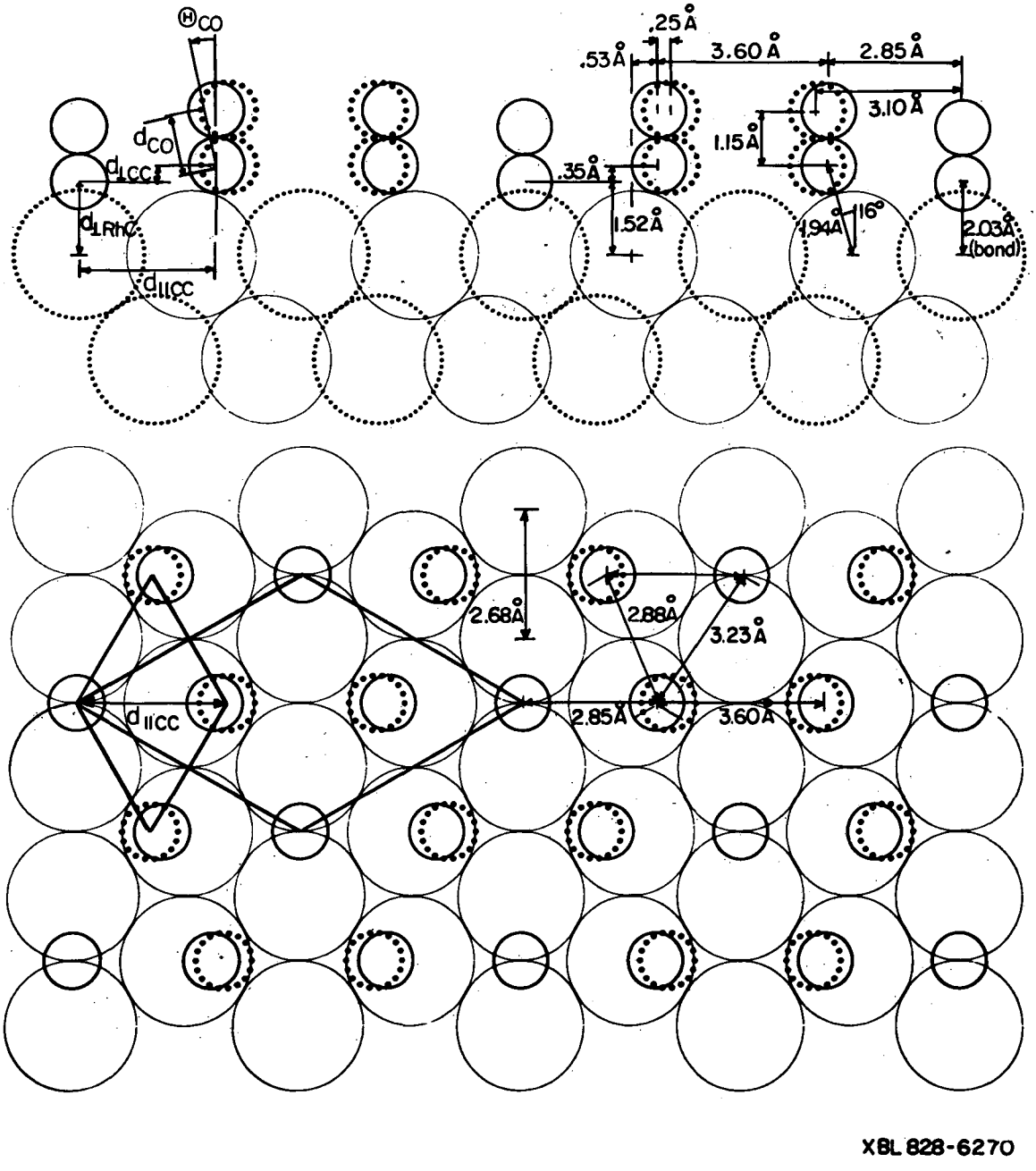
Rh(111) (2×2) - 3 CO
⊕CO
dCO
dLCC
dLRhC
dllCC
.25Å
.53Å
3.60 Å
2.85 Å
3.10 Å
1.15Å
.35Å
1.52Å
1.94Å
16°
2.03Å (bond)
2.68Å
2.88Å
3.23Å
dllCC
2.85Å
3.60Å
XBL 828-6270

Figure 19

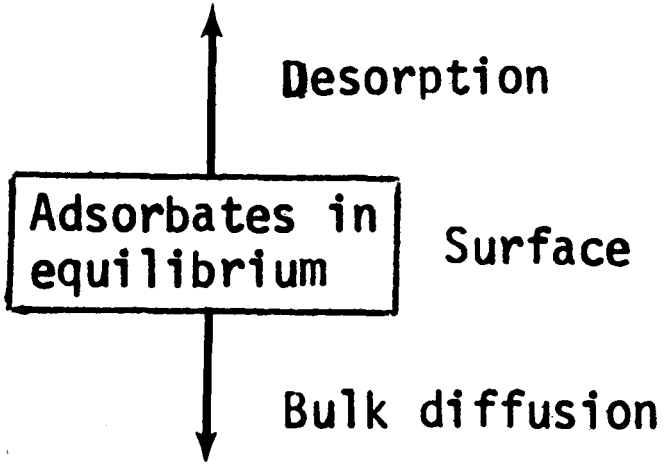

Exceptions: low pressure-high surface temperature studies (molecular beam-surface scattering)
exothermic surface reactions?

XBL 846-2518

Figure 20

Different ethylidyne species: bond distances and angles
(r_C = carbon covalent radius; r_M = bulk metal atomic radius)

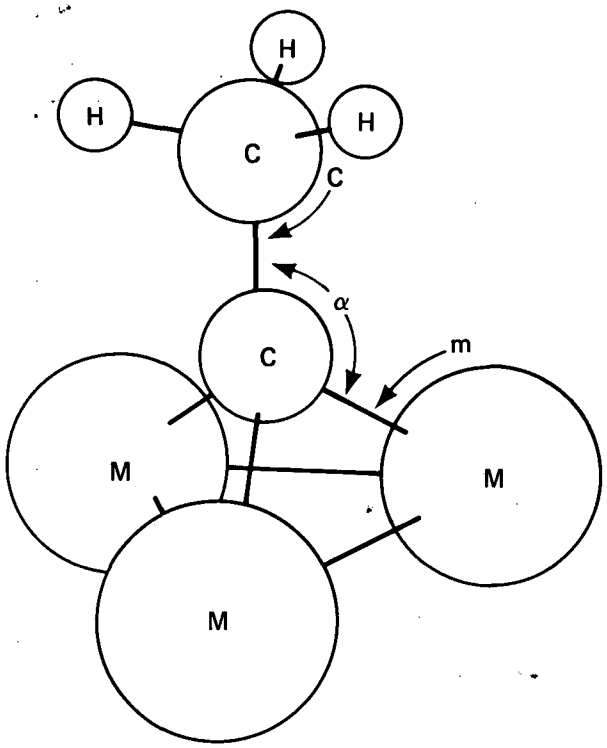

	C [Å]	m	r_M	r_C	α [°]
$Co_3 (CO)_9 CCH_3$	1.53 (3)	1.90 (2)	1.25	0.65	131.3
$H_3 Ru_3 (CO)_9 CCH_3$	1.51 (2)	2.08 (1)	1.34	0.74	128.1
$H_3 Os_3 (CO)_9 CCH_3$	1.51 (2)	2.08 (1)	1.35	0.73	128.1
Pt (111) + (2 × 2) CCH_3	1.50	2.00	1.39	0.61	127.0
Rh (111) + (2 × 2) CCH_3	1.45 (10)	2.03 (7)	1.34	0.69	130.2
$H_3C - CH_3$	1.54			0.77	109.5
$H_2C = CH_2$	1.33			0.68	122.3
$HC \equiv CH$	1.20			0.60	180.0

XBL 818-11196

Figure 21

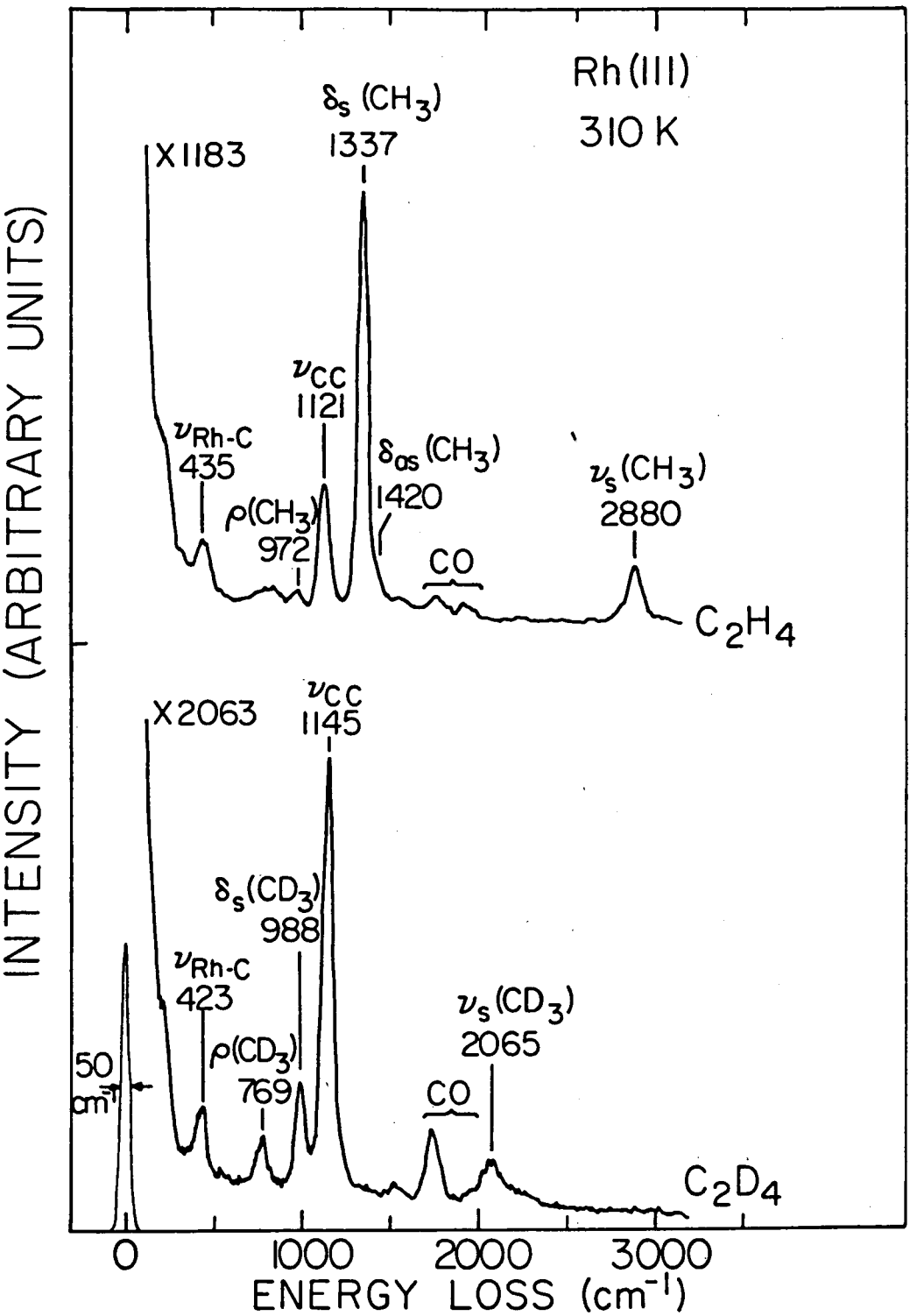

XBL 838-6209

Figure 22

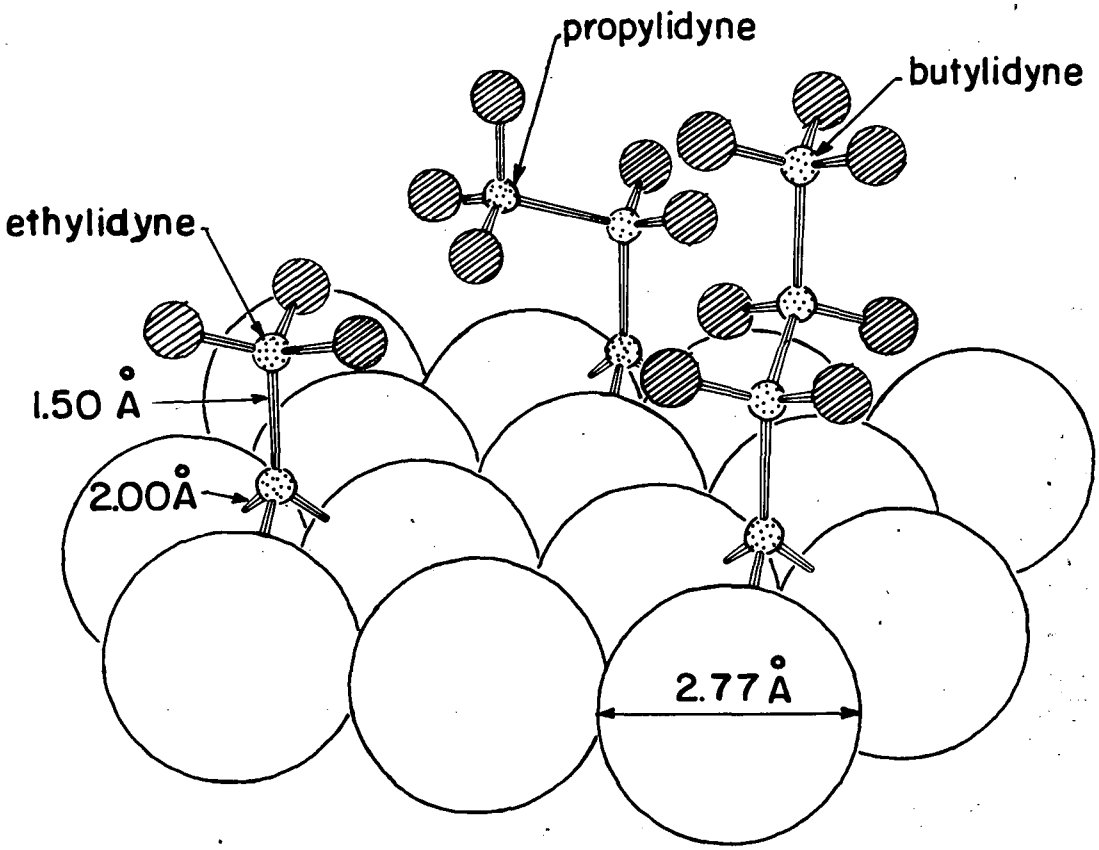

Pt(111) + ethylidyne, propylidyne and butylidyne

XBL 8110-6882

Figure 23

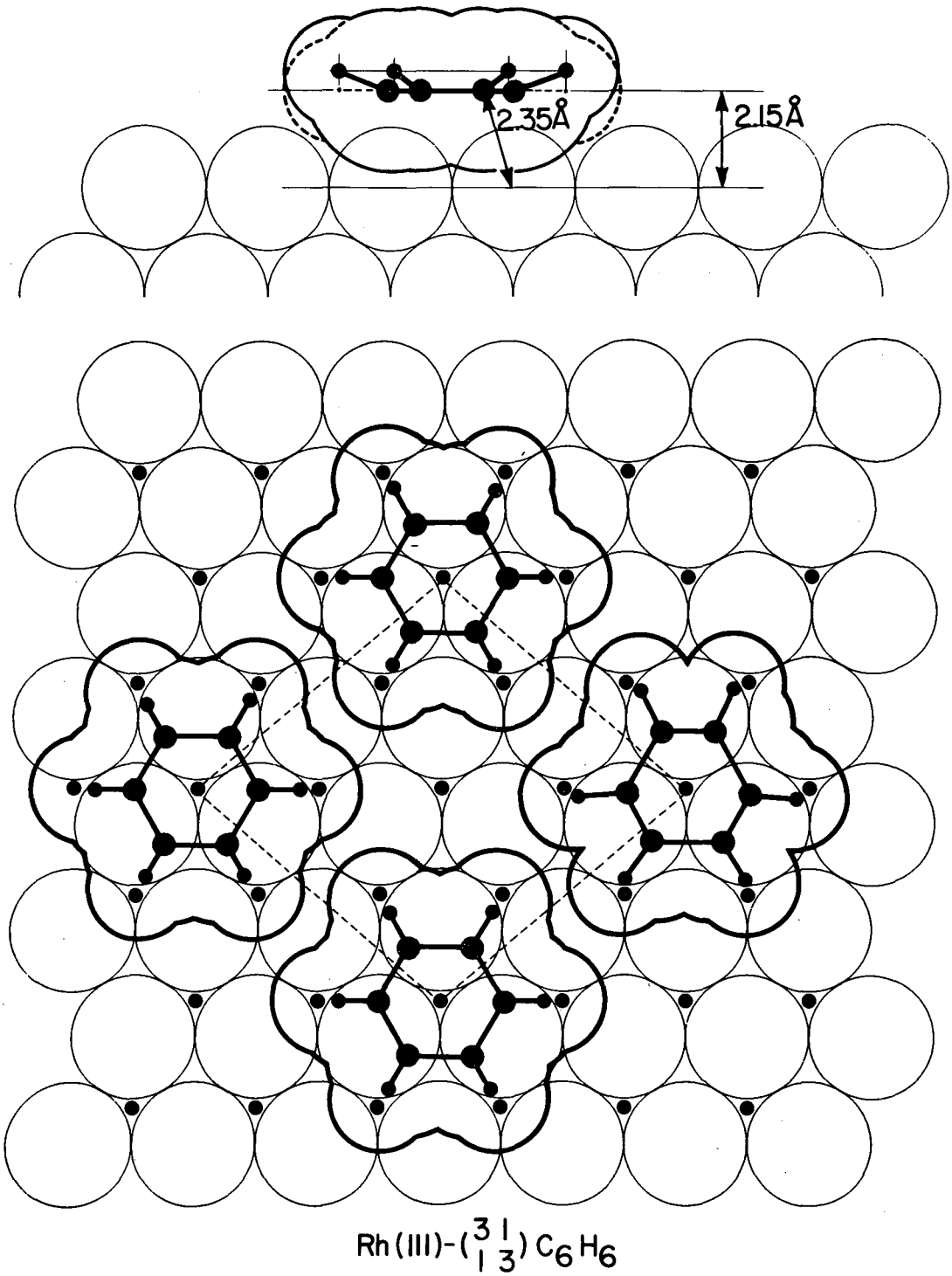

XBL 835-198

Figure 24

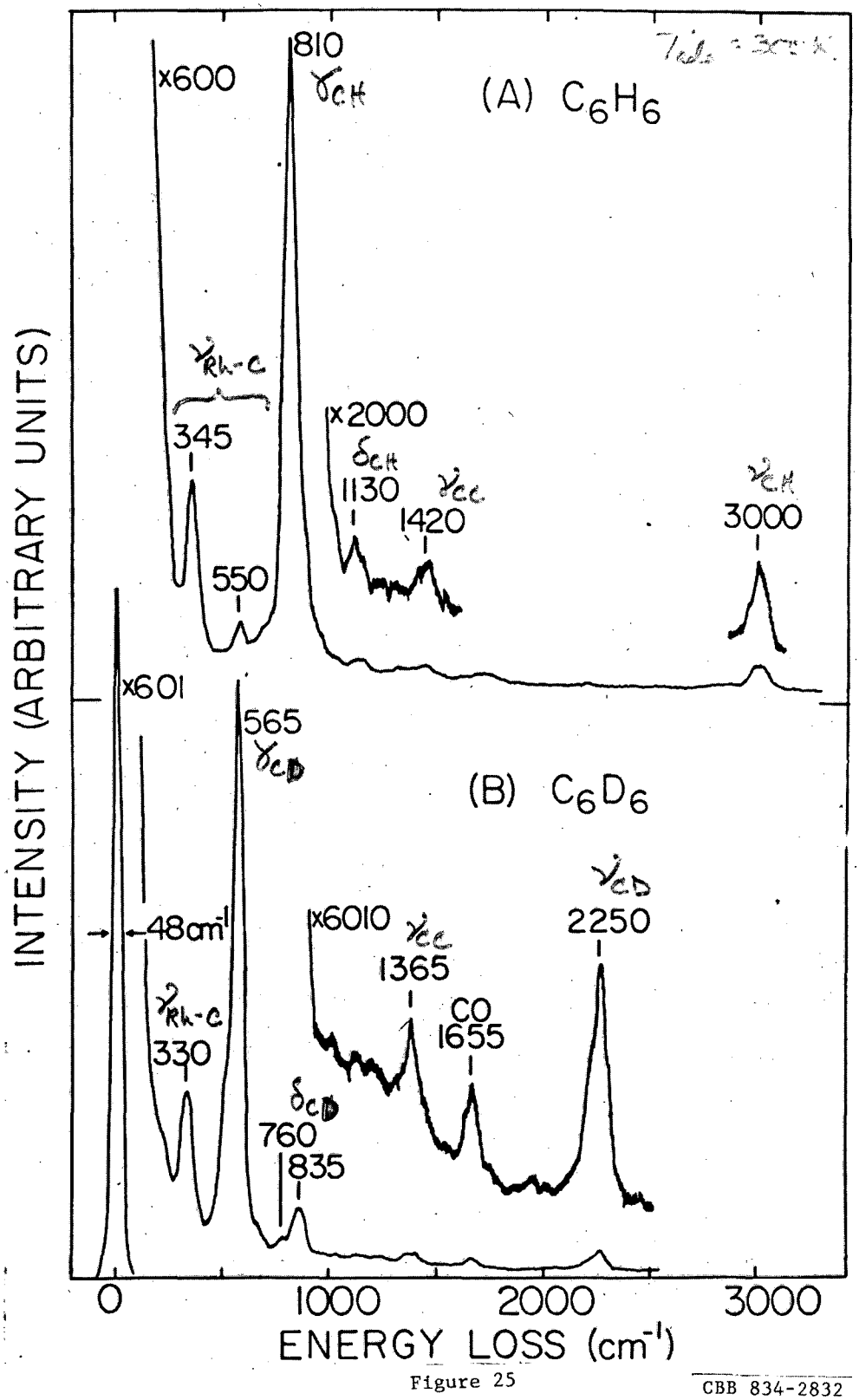

Figure 25

CBB 834-2832

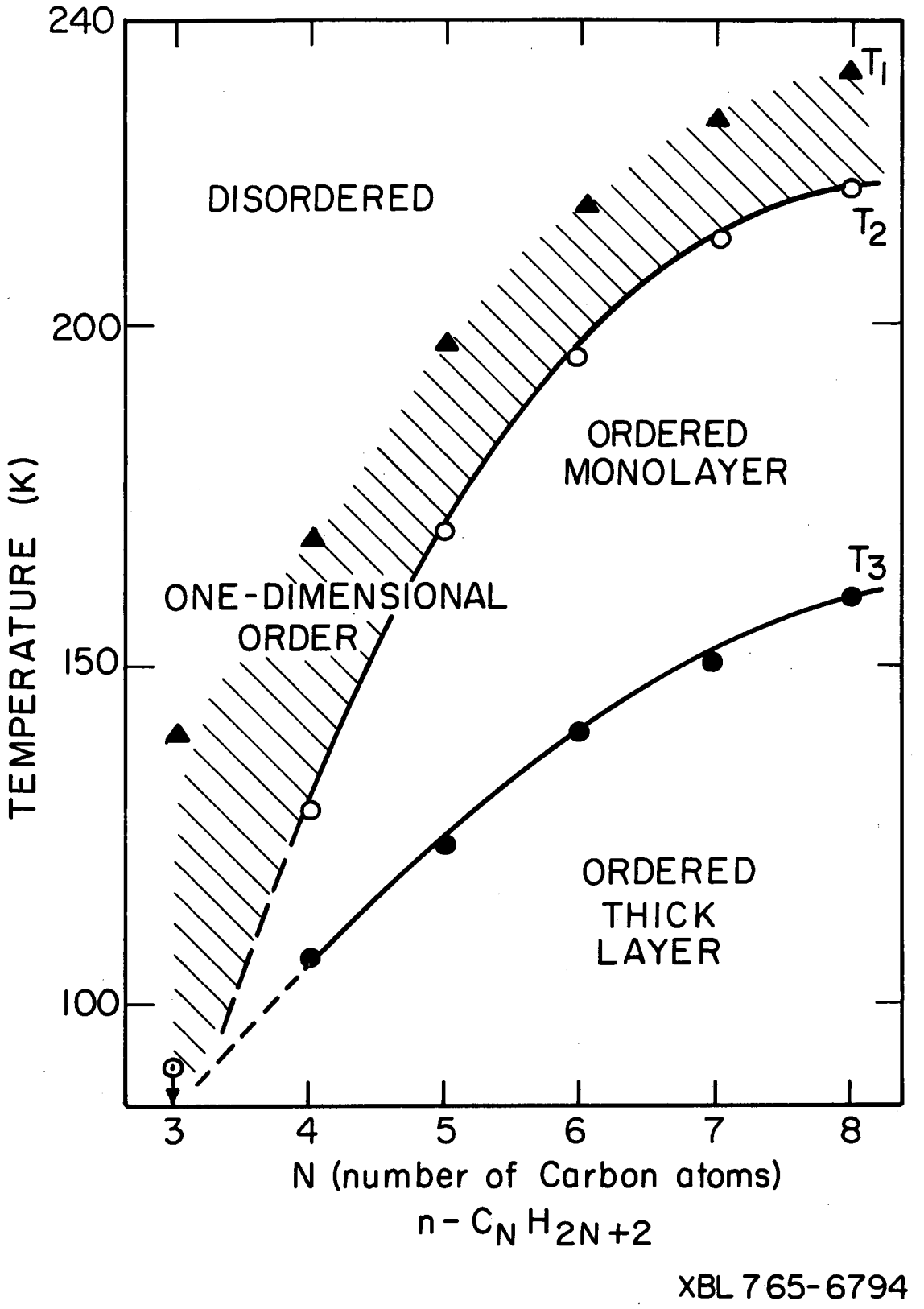
240
200
150
100
TEMPERATURE (K)
DISORDERED
ORDERED
MONOLAYER
ONE-DIMENSIONAL
ORDER
ORDERED
THICK
LAYER
T1
T2
T3
3
4
5
6
7
8
N (number of Carbon atoms)
n - CN H2N+2
XBL 765-6794

Figure 26

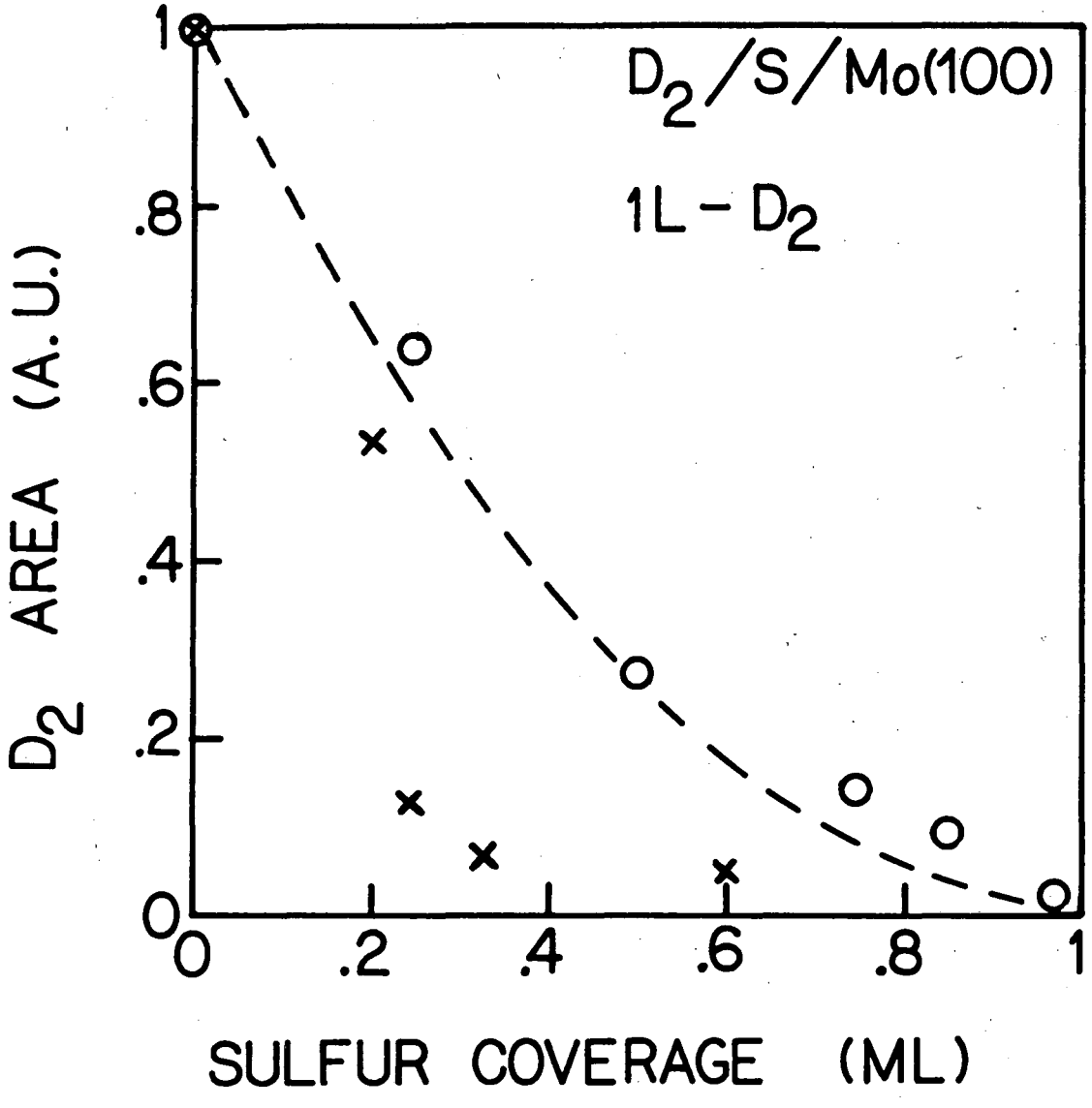

XBL 837-10689

Figure 27

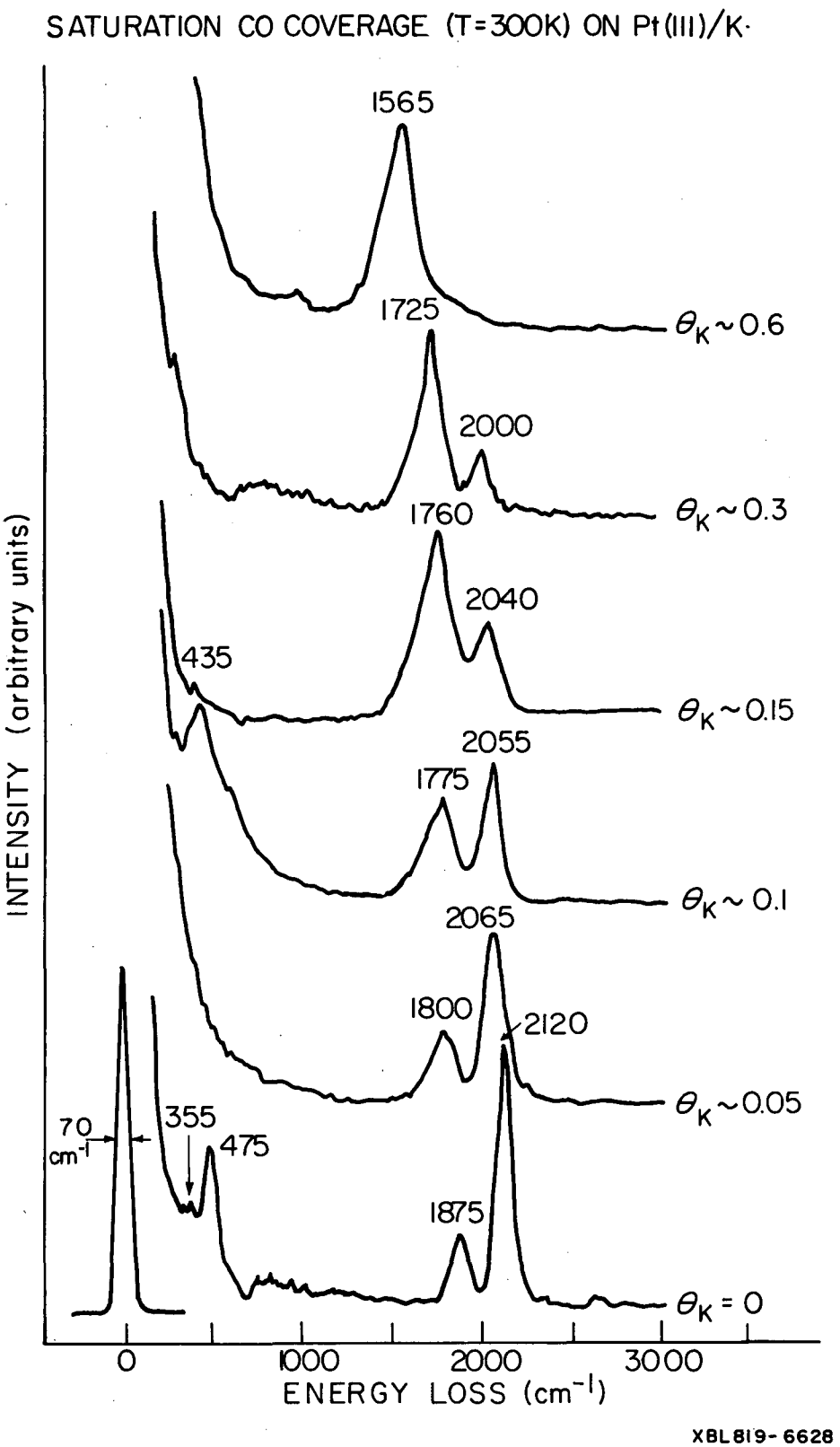
SATURATION CO COVERAGE (T=300K) ON Pt(111)/K
1565
1725
$\theta_K \sim 0.6$
2000
$\theta_K \sim 0.3$
1760
2040
435
$\theta_K \sim 0.15$
2055
1775
$\theta_K \sim 0.1$
2065
1800
2120
$\theta_K \sim 0.05$
70 cm^{-1}
355
475
1875
$\theta_K = 0$
INTENSITY (arbitrary units)
0
1000
2000
3000
ENERGY LOSS (cm^{-1})
XBL819-6628

Figure 28

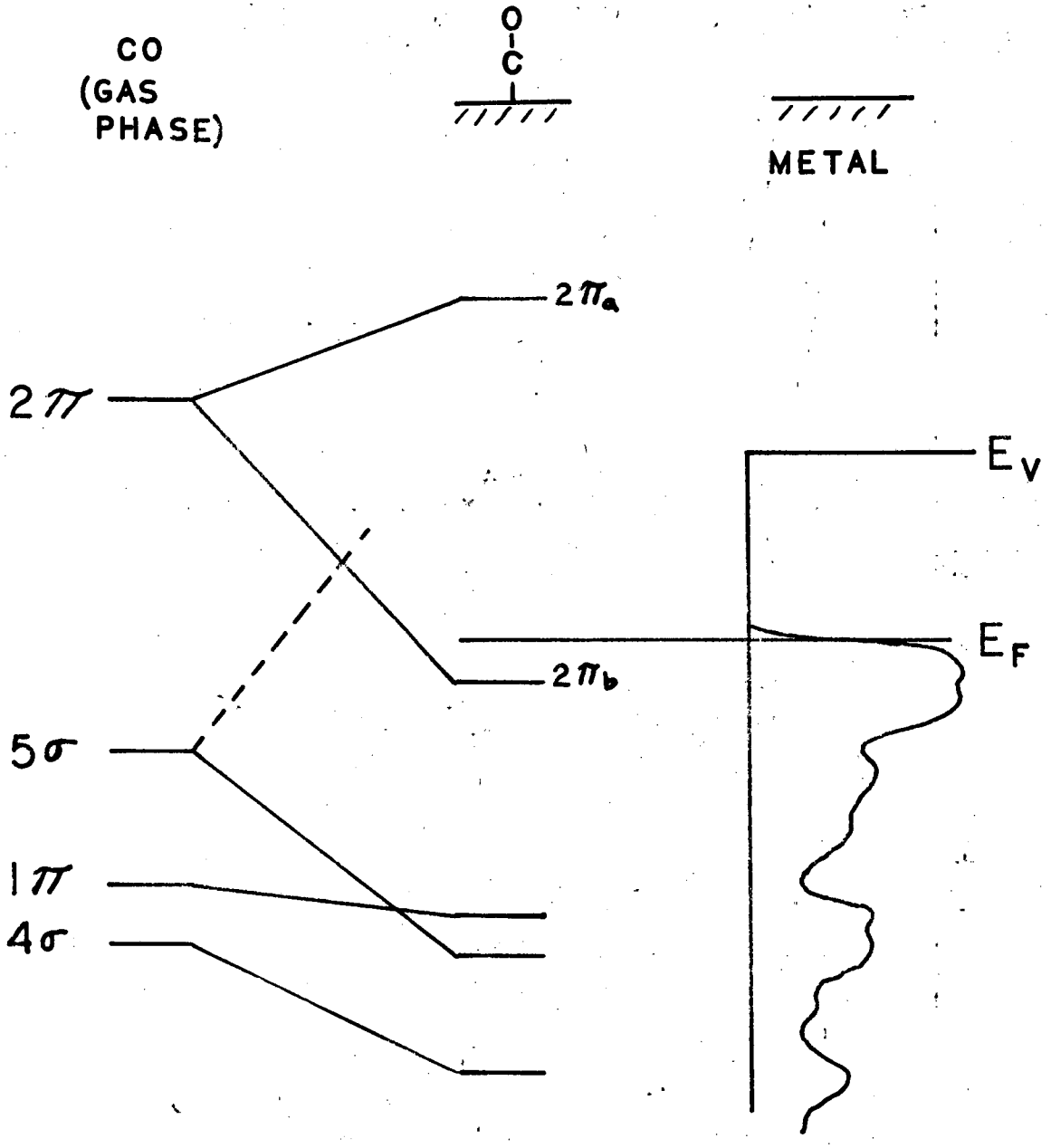

CO BONDING TO METALS

XBL 838-11077

Figure 29

Plot of number of CO molecules that dissociate per potassium as a function of potassium coverage.

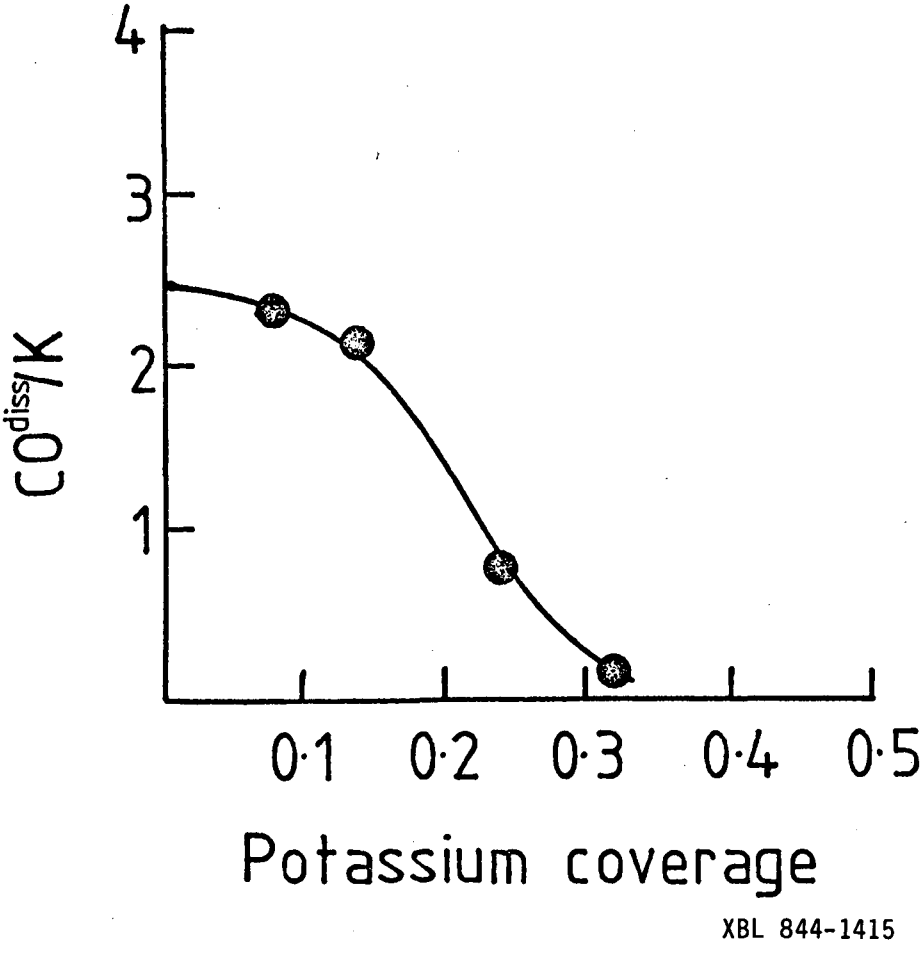

Figure 30

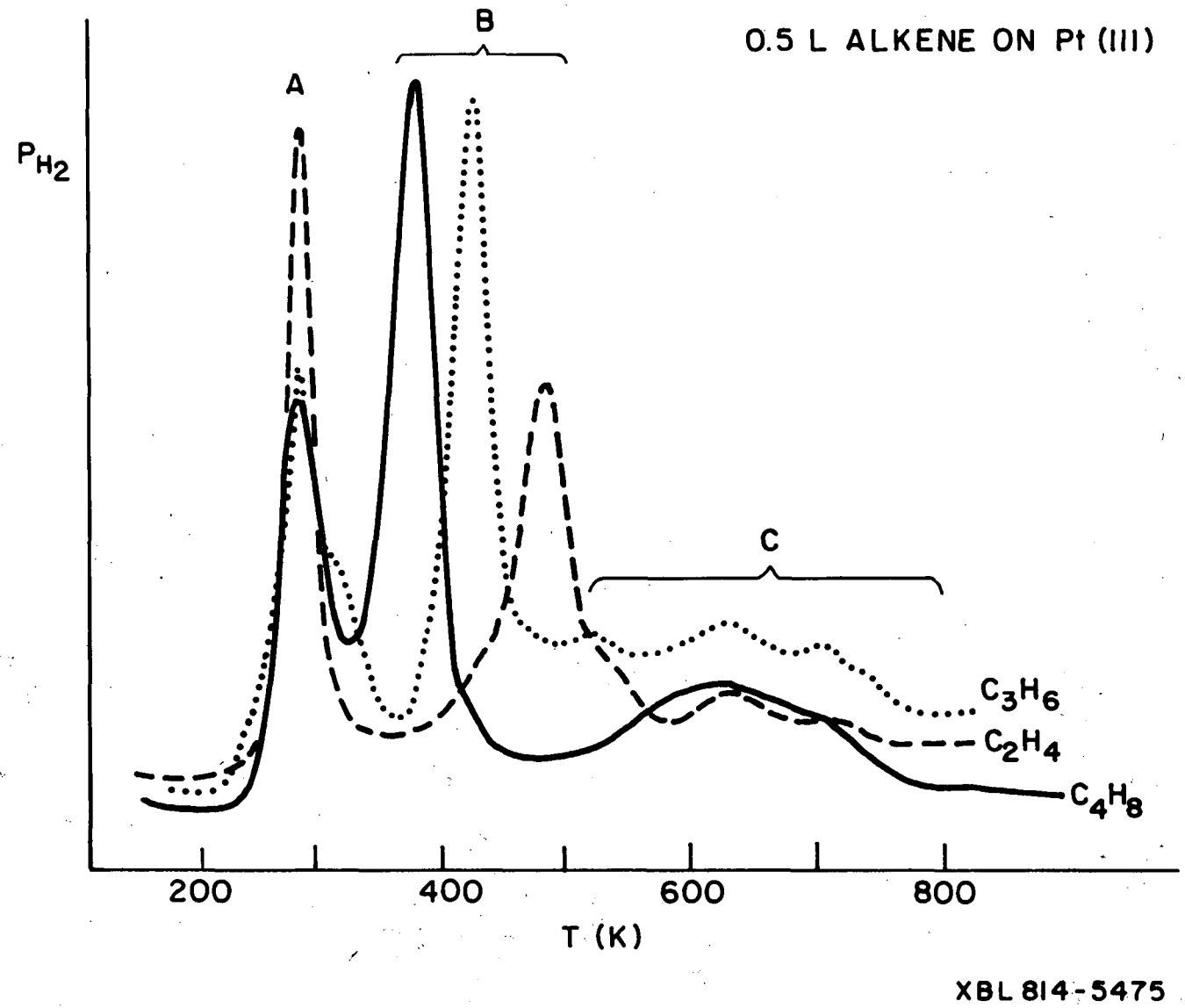
0.5 L ALKENE ON Pt (111)
A
B
C
P_{H_2}
C_3H_6
C_2H_4
C_4H_8
200
400
600
800
T (K)
XBL 814-5475

Figure 31

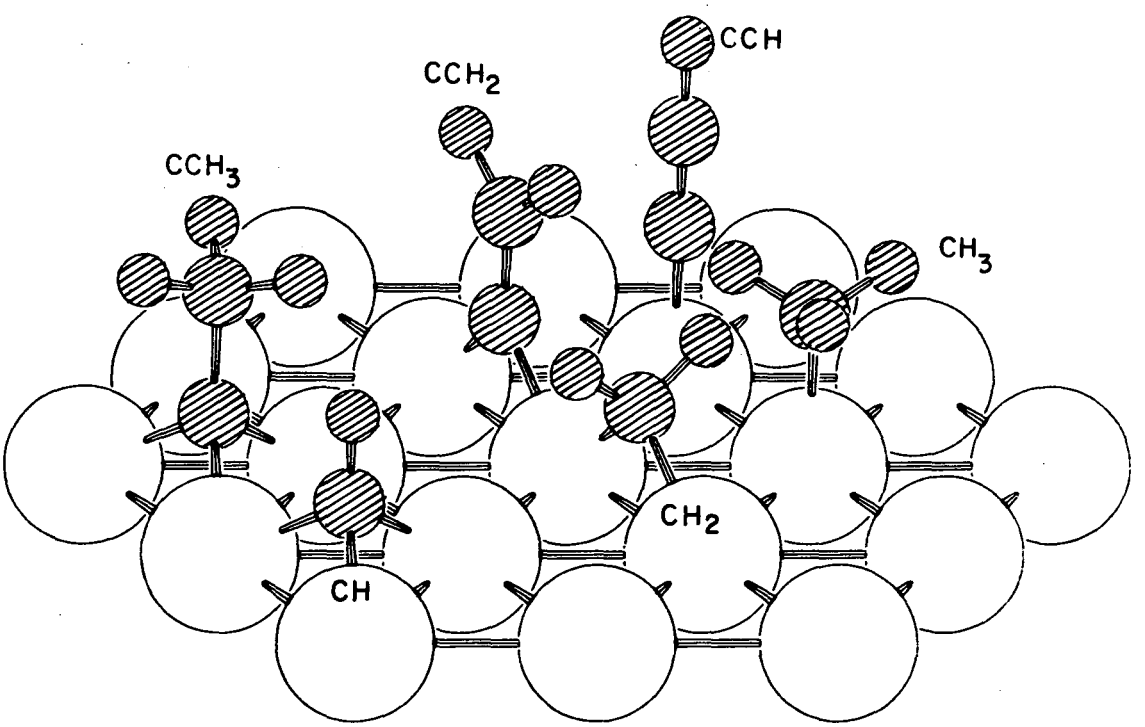

XBL 826-5941

Figure 32

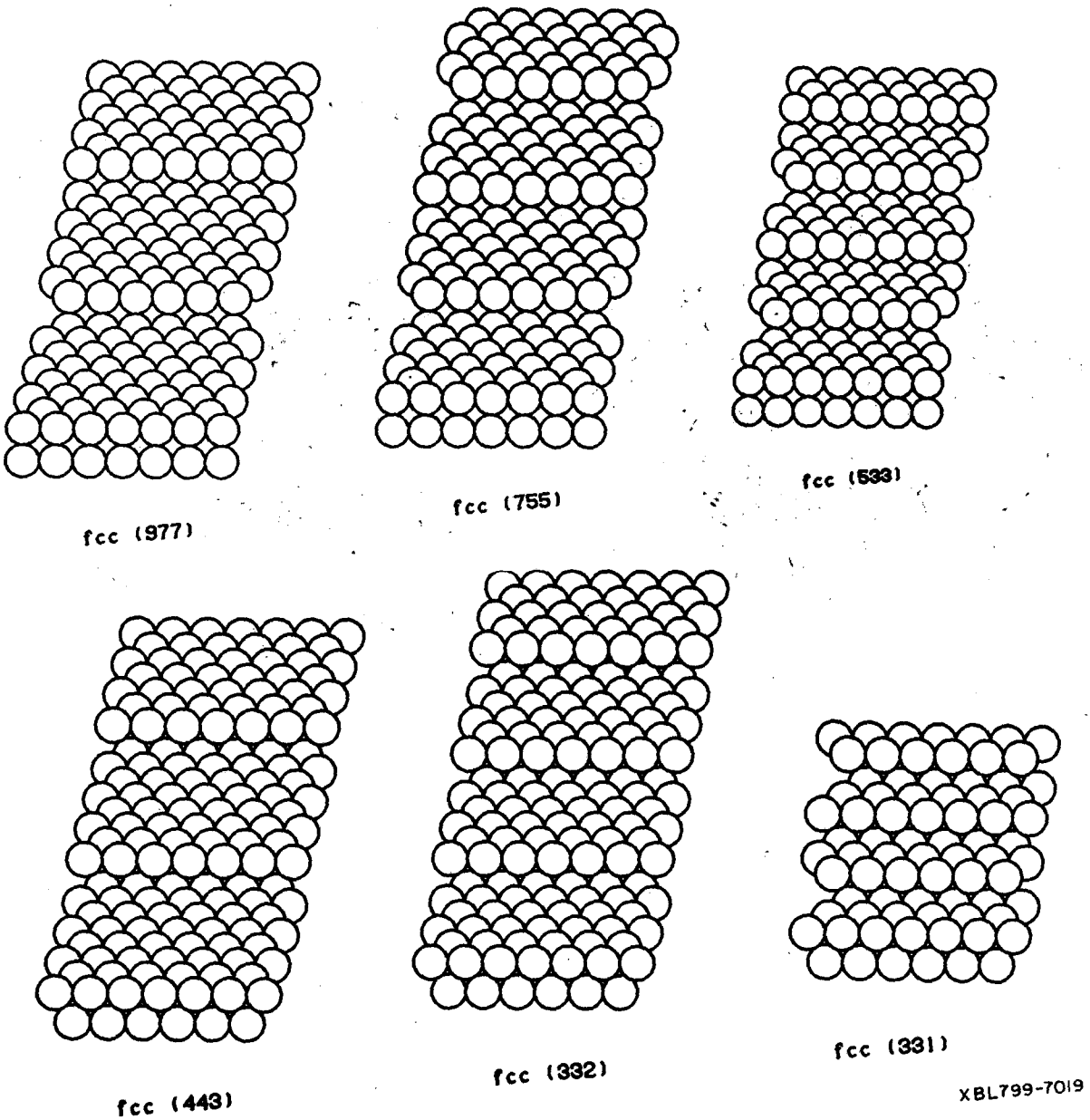

Figure 33

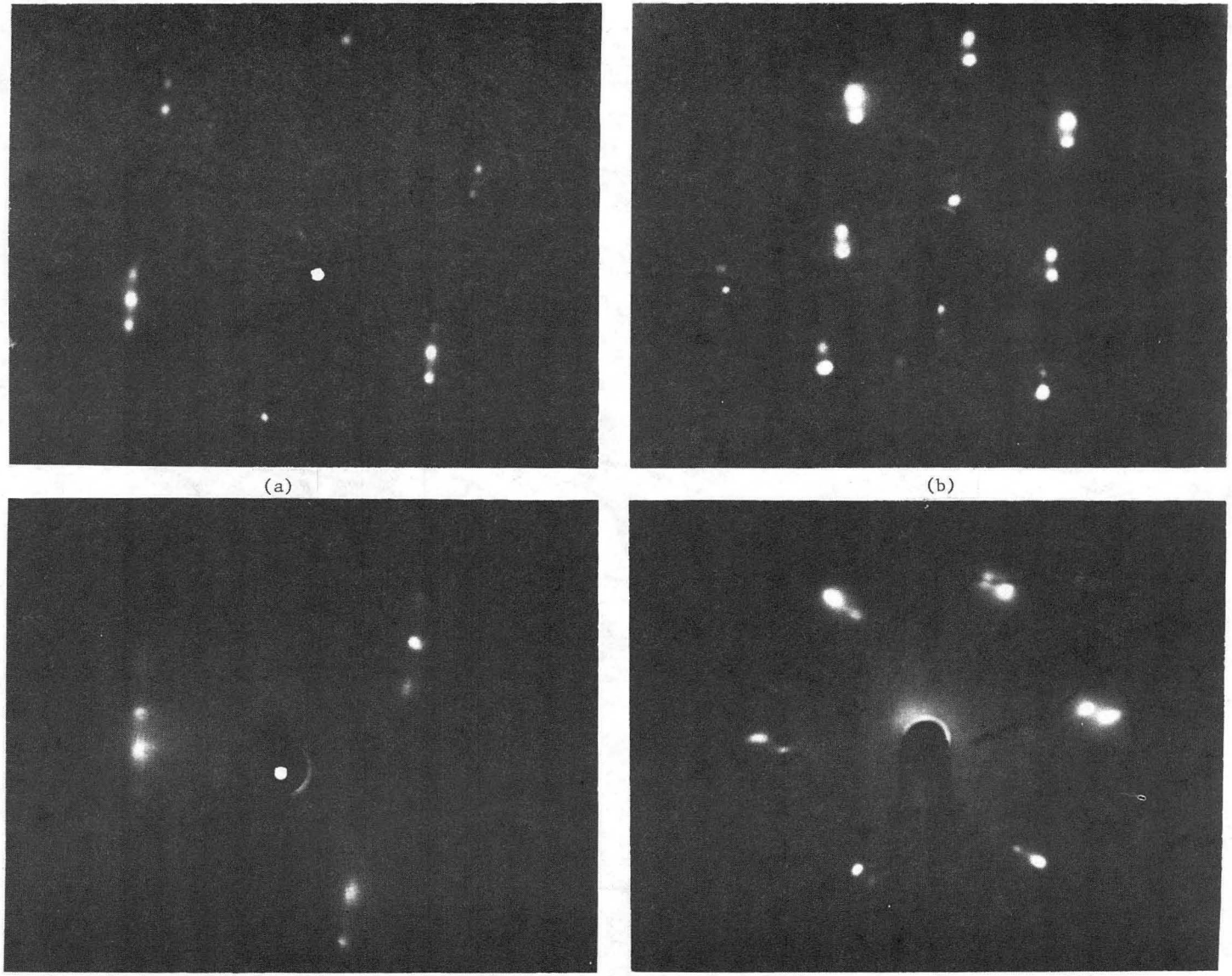

(a) (b) (c) (d)

Figure 34

XBB 733-1571

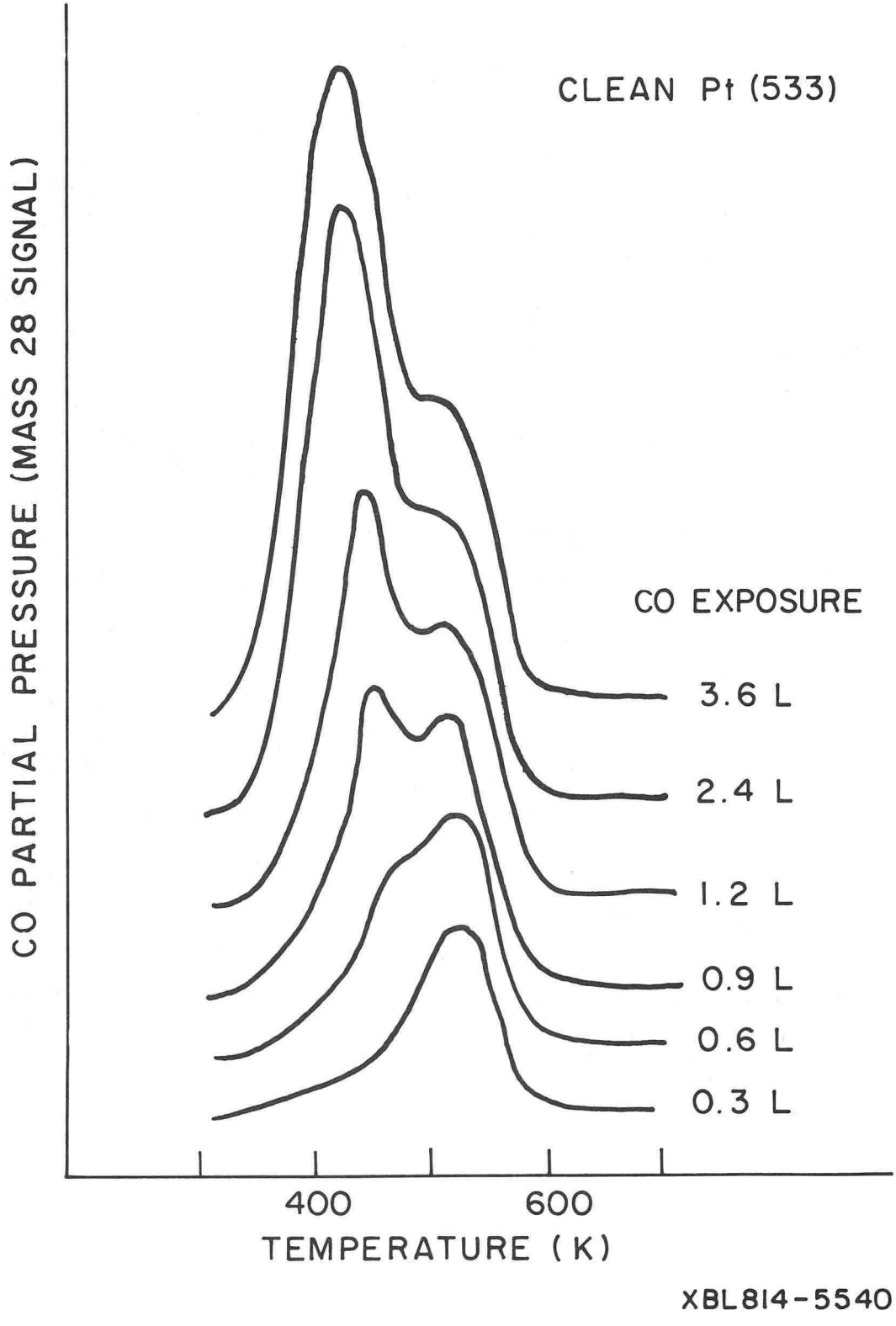
CLEAN Pt (533)
CO EXPOSURE
3.6 L
2.4 L
1.2 L
0.9 L
0.6 L
0.3 L
CO PARTIAL PRESSURE (MASS 28 SIGNAL)
400
600
TEMPERATURE (K)
XBL814-5540

Figure 35

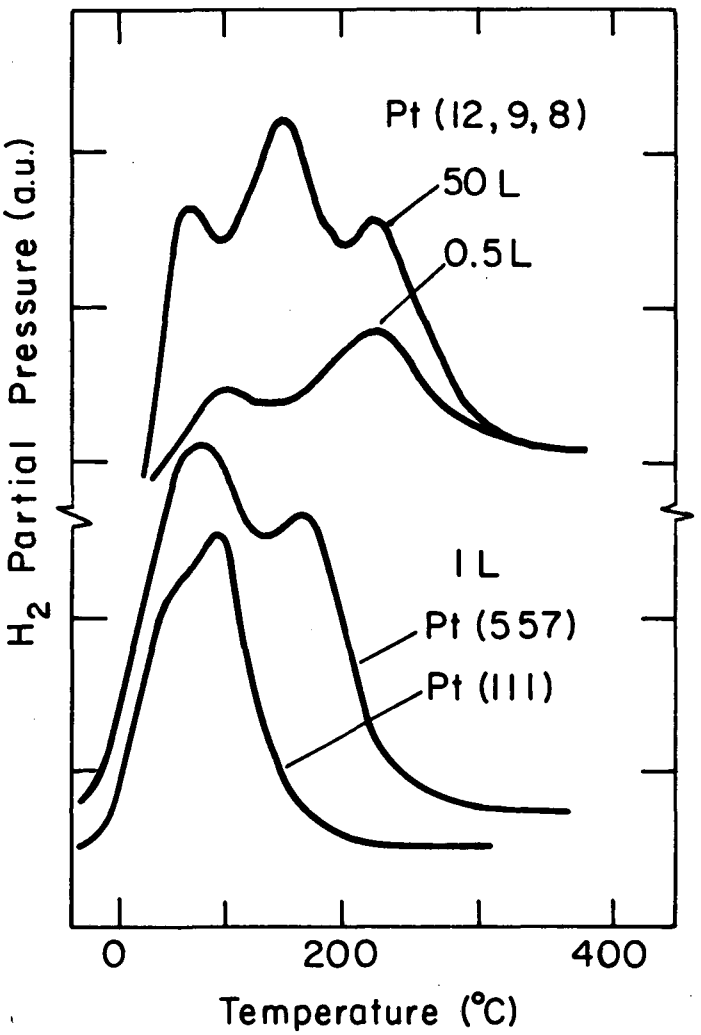

XBL 792-5816

Figure 36

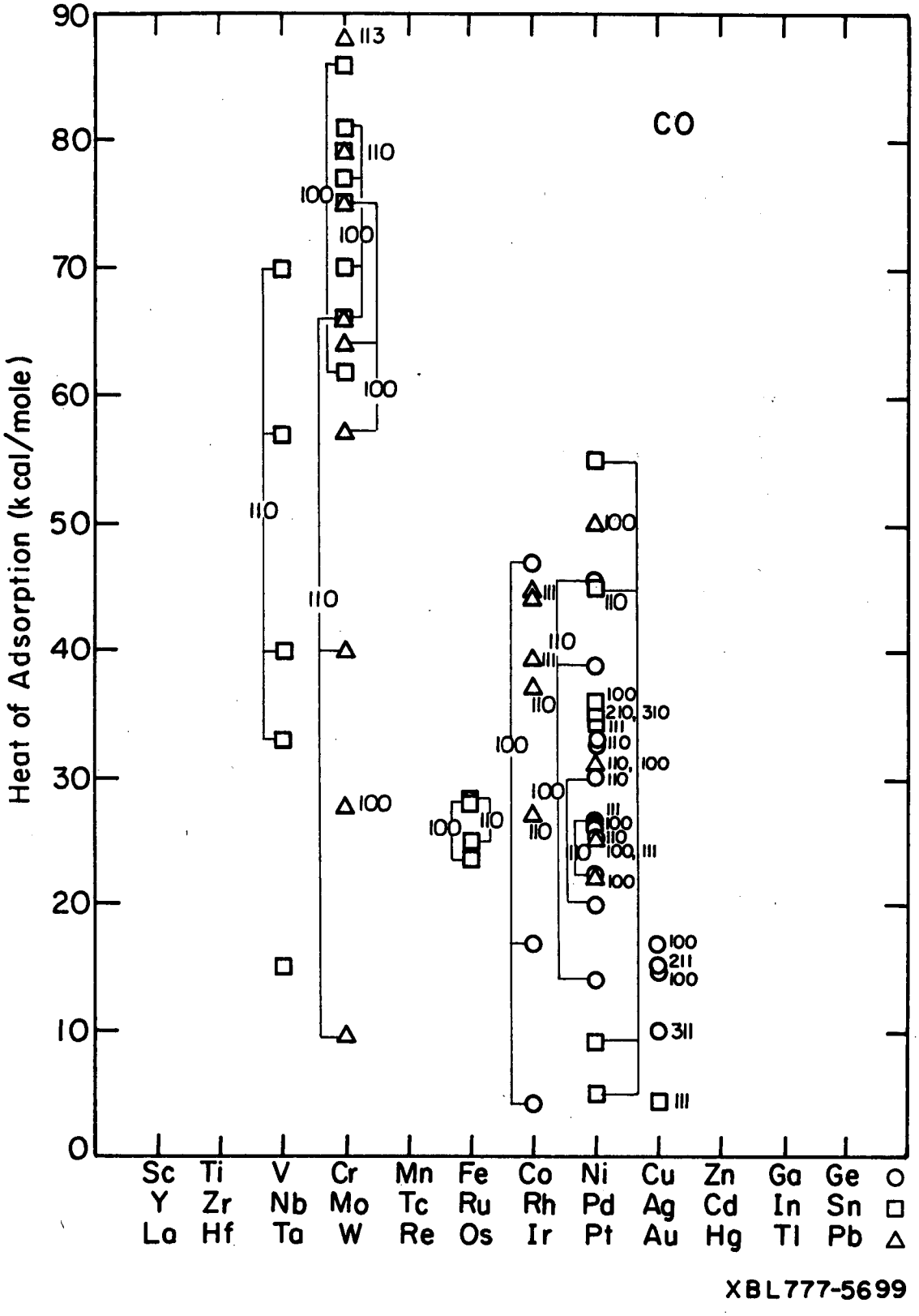
CO
Heat of Adsorption (kcal/mole)
0
10
20
30
40
50
60
70
80
90
Sc Ti V Cr Mn Fe Co Ni Cu Zn Ga Ge
Y Zr Nb Mo Tc Ru Rh Pd Ag Cd In Sn
La Hf Ta W Re Os Ir Pt Au Hg Tl Pb
XBL777-5699

Figure 37

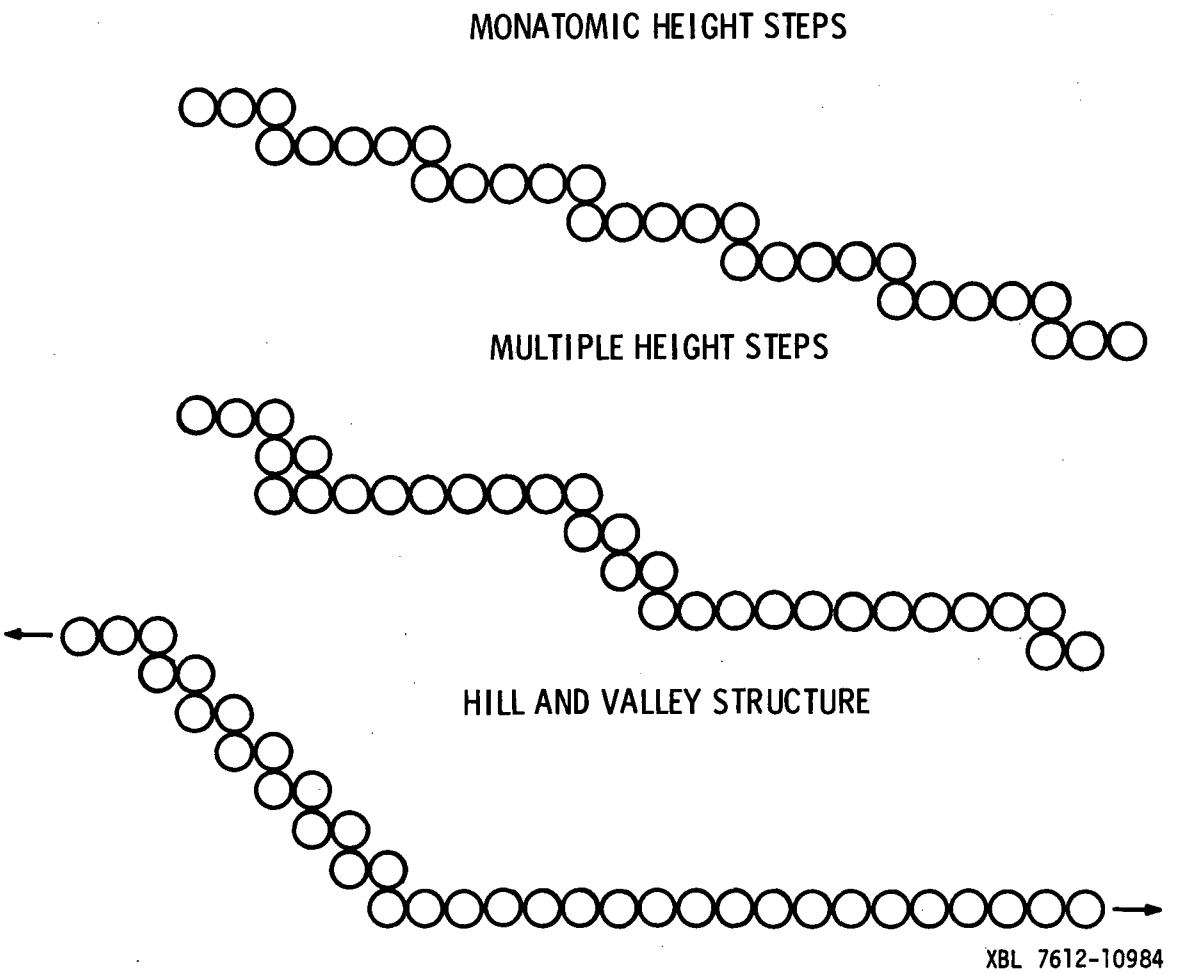
MONATOMIC HEIGHT STEPS
MULTIPLE HEIGHT STEPS
HILL AND VALLEY STRUCTURE
XBL 7612-10984

Figure 38

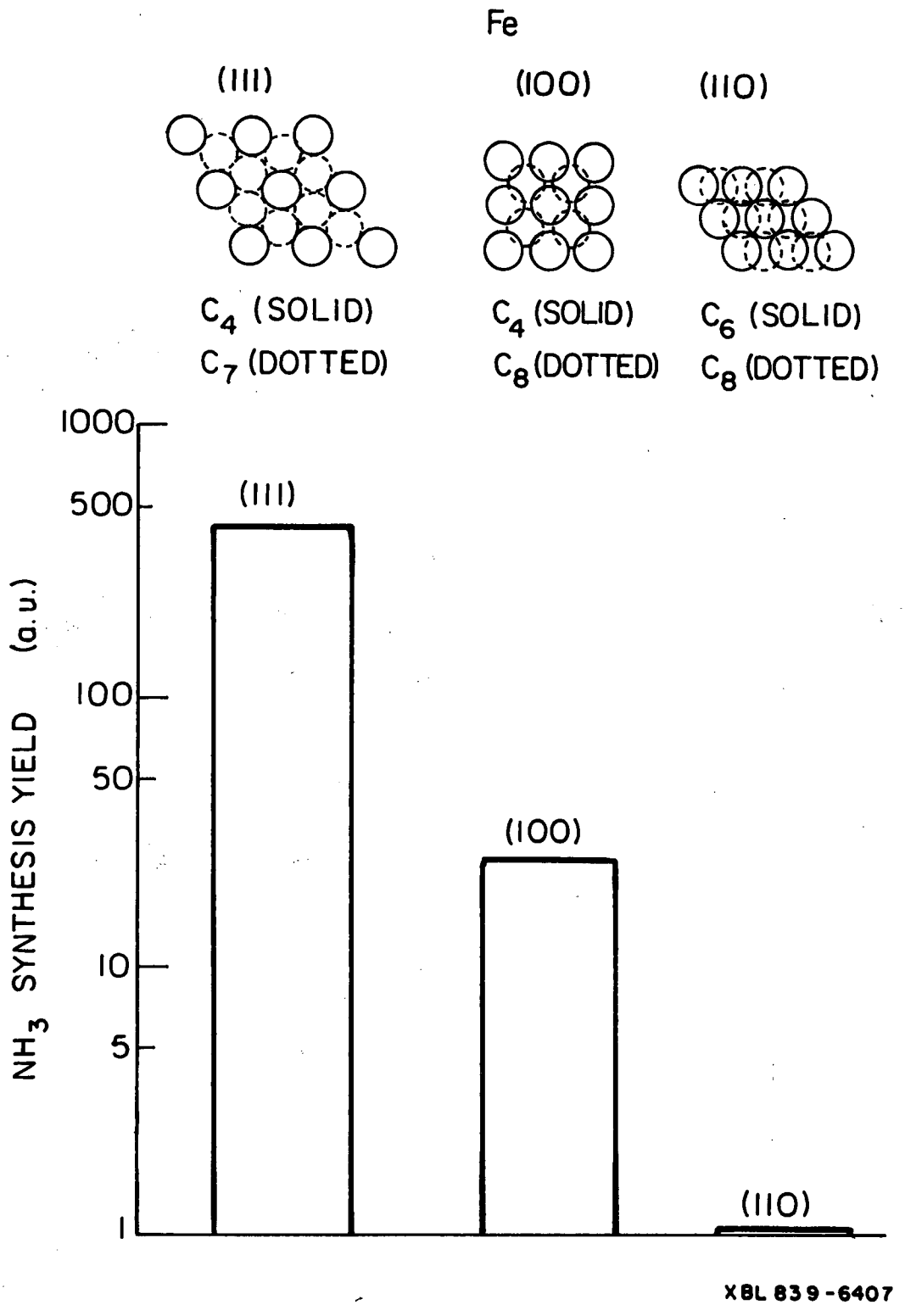
Fe
(111)
(100)
(110)
C_4 (SOLID)
C_7 (DOTTED)
C_4 (SOLID)
C_8 (DOTTED)
C_6 (SOLID)
C_8 (DOTTED)
1000
500
100
50
10
5
1
NH_3 SYNTHESIS YIELD (a.u.)
(111)
(100)
(110)
XBL 839-6407

Figure 39

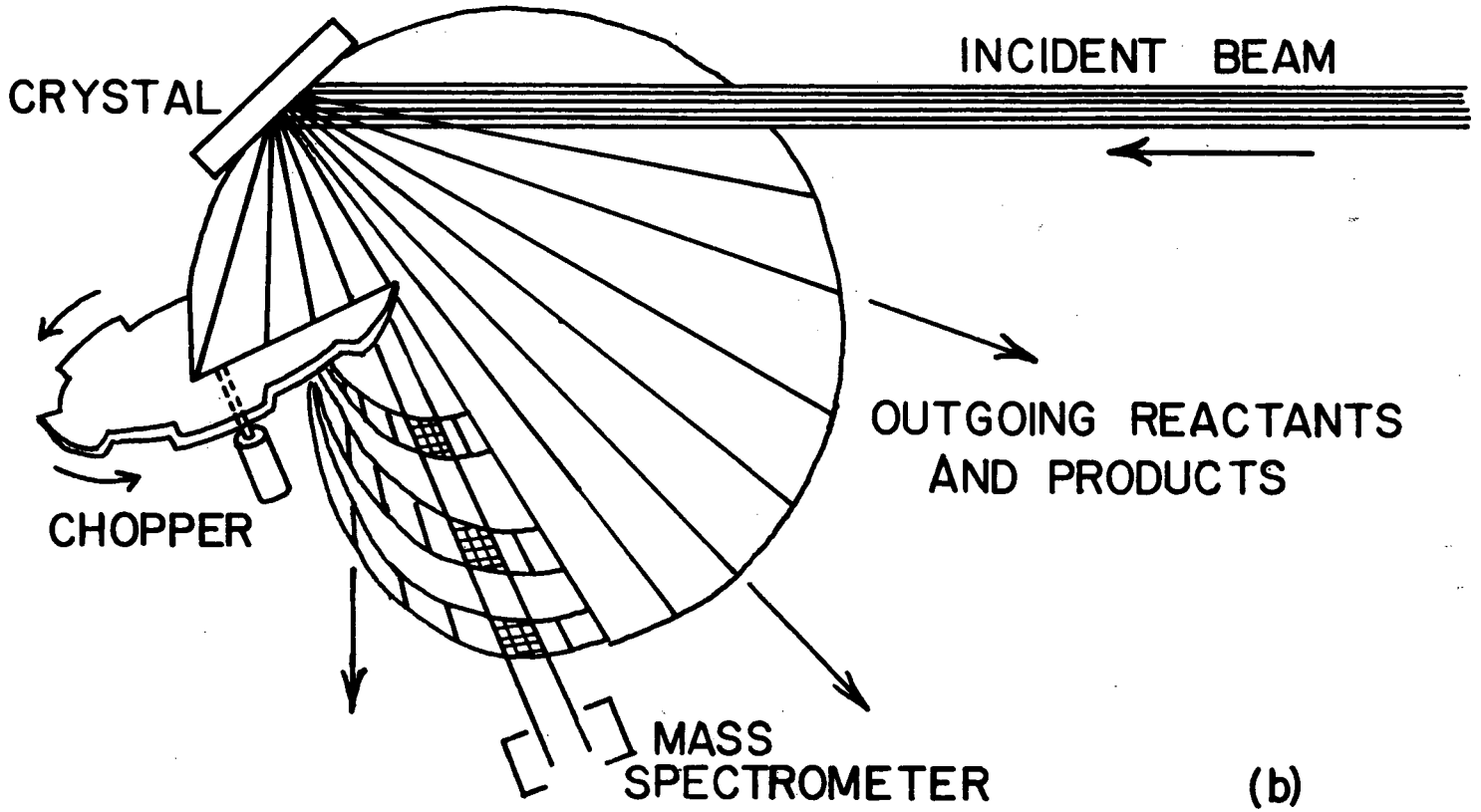
CRYSTAL
INCIDENT BEAM
OUTGOING REACTANTS
AND PRODUCTS
CHOPPER
MASS
SPECTROMETER
(b)
XBL 812-8100

Figure 40

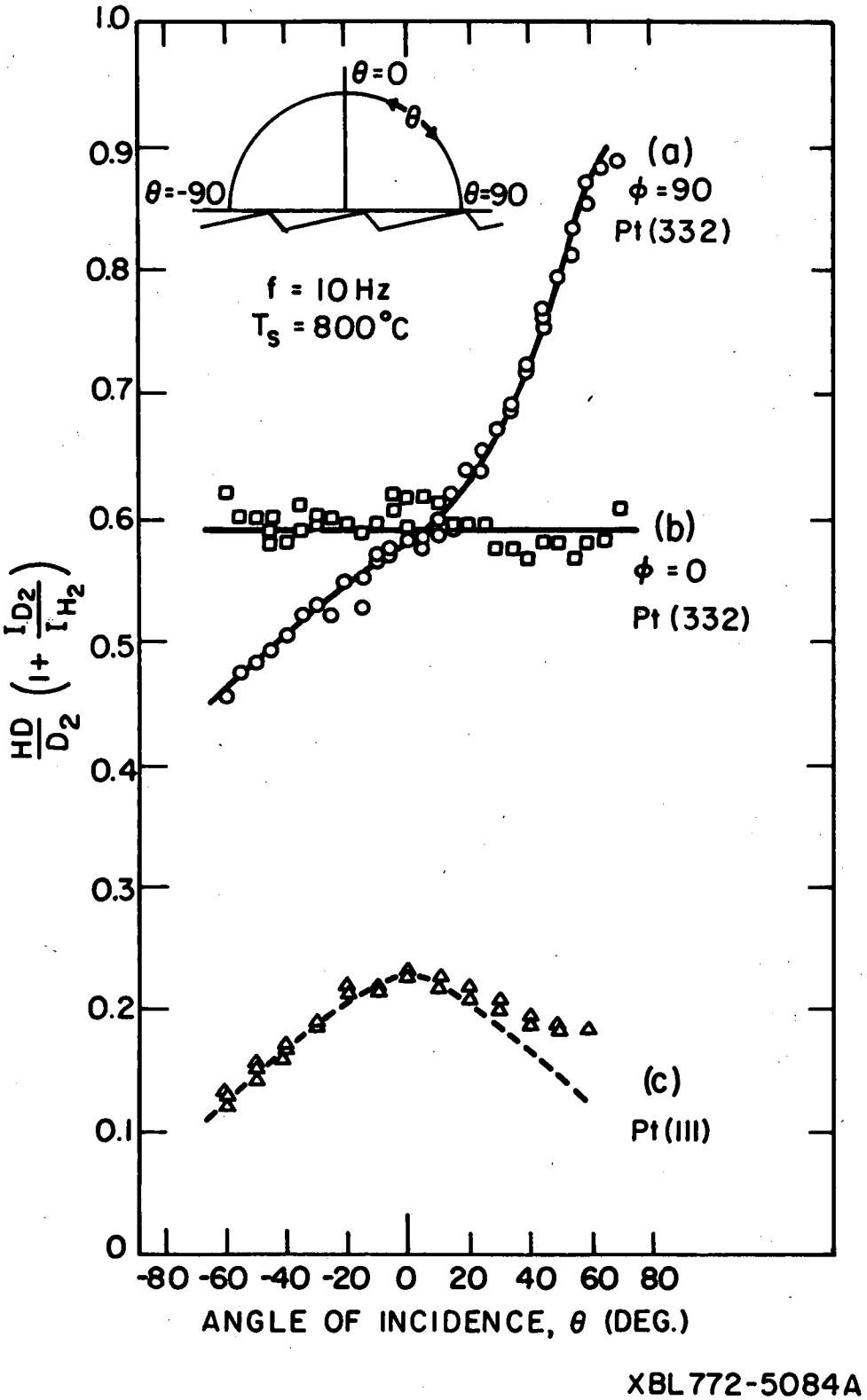
1.0
0.9
0.8
0.7
0.6
0.5
0.4
0.3
0.2
0.1
0
θ=0
θ
θ=-90
θ=90
(a)
φ=90
Pt(332)
f = 10 Hz
T_s = 800°C
(b)
φ=0
Pt(332)
(c)
Pt(111)
HD/D2 (1 + I_D2/I_H2)
-80 -60 -40 -20 0 20 40 60 80
ANGLE OF INCIDENCE, θ (DEG.)
XBL772-5084A

Figure 41

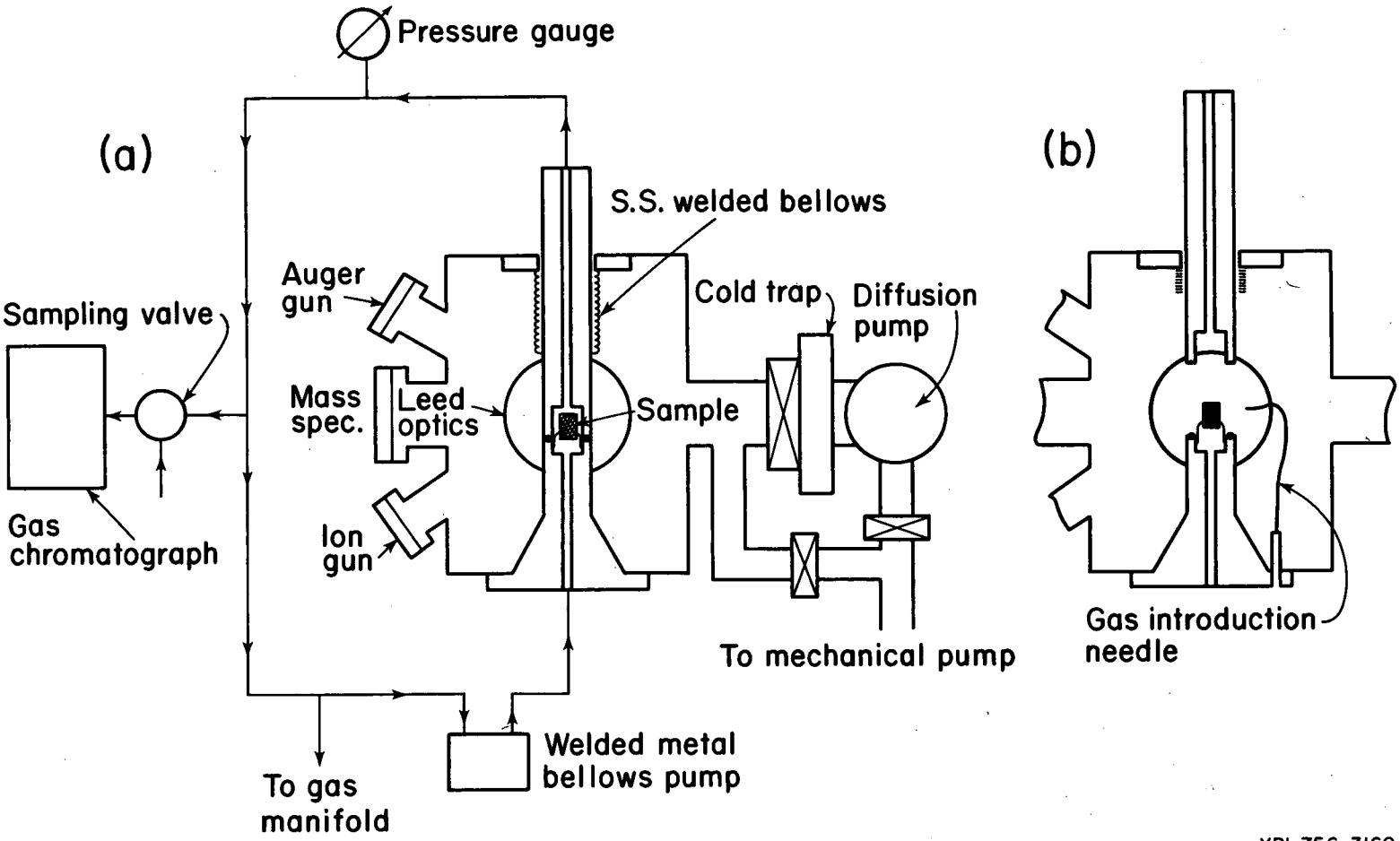
(a)
Pressure gauge
S.S. welded bellows
Auger gun
Cold trap
Diffusion pump
Sampling valve
Mass spec.
Leed optics
Sample
Gas chromatograph
Ion gun
To mechanical pump
Welded metal bellows pump
To gas manifold
(b)
Gas introduction needle
XBL 756-3160

Figure 42

TECHNICAL INFORMATION DEPARTMENT
LAWRENCE BERKELEY LABORATORY
UNIVERSITY OF CALIFORNIA
BERKELEY, CALIFORNIA 94720